

CAUSAL EFFECTS AND PREDICTION OF LAND USE SYSTEMS IN RURAL LANDSCAPES: EVIDENCE FROM HENAN PROVINCE

Isaac Sarfo^{1,2}  0000-0002-6914-5764, Jiajun Qiao¹  0000-0003-3494-2197, Emmanuel Yeboah³  0000-0003-3838-6837, Abraham Okrah^{4,5}  0009-0006-8049-7310, Charafa El Rhadiouini³, Benjamin Kwapong Osibo⁶, Anita Boah⁷, Dhekra Ben Amara¹  0009-0000-2467-8754

¹ College of Geography and Environmental Science, Henan University, Kaifeng city, Henan Province, China

² Organization of African Academic Doctors (OAAD), Off Kamiti Road, P.O. Box 25305000100, Nairobi, Kenya

³ School of Remote Sensing and Geomatics Engineering, Nanjing University of Information Science and Technology, 210044 Nanjing, Jiangsu, China

⁴ Collaborative Innovation Center on Forecast and Evaluation of Meteorological Disaster, Nanjing University of Information Science and Technology, 210044 Nanjing, Jiangsu, China

⁵ Department of Meteorology and Climate Science, Kwame Nkrumah University of Science and Technology, 00233, Kumasi, Ghana

⁶ School of Computer and Software, Nanjing University of Information Science and Technology, 210044 Nanjing, Jiangsu, China

⁷ Department of Public Health and Allied Sciences, Catholic University, Fiapre, Ghana

ABSTRACT

Aim of the study

In rural and agricultural development, land plays a crucial role in driving productivity. To understand the impact of specific causes or combinations of causes on outcomes, it is essential to identify and establish clear causal relationships. Our study investigates the causal effects of different land use systems against Land Surface Temperature (LST) in Henan Province. We further make land use predictions based on current trends. Understanding these dynamics is essential for enhancing agricultural informatization, environmental management, and climate-smart choices of local districts, counties and villages across China's agriculturally important regions and beyond.

Material and methods

The study utilized integrated remote sensing data, techniques and a causality approach to investigate land use systems (LUS) and LST in Henan Province. We further used Modules for Land Use Change Evaluation (MOLUSCE) and Cellular Automata-Artificial Neural Network (CA-ANN) to predict LUS for the near future (2023–2053).

Results and conclusions

Results revealed that built-up areas (+500%), forests (+50.88%) and water bodies (+83.56%) have expanded massively during the past 40 years. In contrast, cultivated (–20.81%) and barren areas (–60.53%) declined steadily. The temporal causal inference analysis demonstrated a strong convergence between built-up areas and land surface temperature (LST), which substantiates built-up areas' profound impact on LST intensity. The spatial causal inference analysis shows moderate to robust positive indirect cross-mapping relationships between built-up areas ($\rho = 0.63$) and bare land ($\rho = 0.32$) against LST. Land use predictions (2023–2053)

✉ e-mail: jjqiao@henu.edu.cn

show a reduction in areas covered by forests and water bodies, and a reversed trend in cultivated lands. These are particularly important when formulating targeted policy-directives needed to regulate unsustainable land-use processes and undesirable economic trade-offs.

Keywords: causal analysis, Geodetector, land use and land cover, land surface temperature (LST), China

INTRODUCTION

In the face of multiple climate stressors, land use systems development (LUSD) plays an essential role in addressing concerns related to land degradation, rural-urban resilience, and the optimal land resource use (Wang et al., 2021). Changes in land use systems continue to be the most fundamental and significant landscape feature that demonstrates human activities' ever-changing impact on the environment. Land systems are the interactions and responses of different key players, institutions, cultural traditions, and competing interests (Turner, 2020). According to Magliocca et al. (2023), one important aspect of land system science (LSS) is the understanding of the driving processes of land use change (LUC). However, the intricate interplay between various elements of different sizes frequently results in complex causality pathways, making it difficult to identify and evaluate causal effects and processes. This phenomenon is critical to understanding local, regional, and global environmental shifts (Reay, 2020). Throughout history, the transition from undisturbed to cultivated areas has been the primary driver of global land use and land cover change (LULCC) (FAO, 2020). In their study titled "Worldwide research trends on sustainable land-use in agriculture," Aznar-Sánchez et al. (2019) found that 42% of the global population relies on agriculture for their livelihood. Many developing countries' economies rely heavily on this industry. Previous studies have shown that when the human population grows at a high rate, so does the demand to convert and use land for agriculture and other purposes. In recent years, there has been a growing focus on studying the sustainable use of land in agriculturally-oriented regions. These regions play an essential role in ensuring food security and economic development, not just in China but also in other parts of the world (Hinz et al., 2020; Xi et al., 2023).

Land use predictions, according to Xu et al. (2022), inform the decisions of city planners, provincial, dis-

trict, and other administrative bodies, among other interested parties, to optimize current efforts aimed at averting undesirable consequences or building resilience against unforeseeable events. In Central China, particularly in Henan province, which contributes immensely to the nation's food basket and economy, a comprehensive understanding of the driving mechanisms through this causality study will provide the much-needed technical basis that supports the sustainable utilization of land and the management of the province's rural (i.e., agricultural areas) and urban settings. Notable solutions among the commonly used predictive land use models in human, regional, and economic geographies include the CA-Markov model (Xu et al., 2022), the GEOMOD model (Sakieh and Salmanmahiny, 2016), the MLP – NN model (Girma et al., 2021), the CLUE-S model (Huang et al., 2019), and the CA-ANN model (Değermenci, 2023). Nevertheless, these standardized models are efficient in modelling trends over a given period. However, each model has some limitations linked to spatial levels, duration/extent of coverage, number of images, as well as ease/convenience and accuracy of modelling. To this end, this study employs a Geodetector and a CA-ANN to investigate and predict the driving mechanisms behind Henan province's LULCC and LST, respectively. It is worth noting that the core and potential drivers, thus, spatial and non-spatial factors of LULCC emanate from different sources. The latter is mainly driven by policy-driven and planning initiatives, which we attempt to explore extensively in this study. Similarly, we focus on the applicability of causality and simulation of future land use systems in an agriculturally-driven region such as the Henan province, which remains underdeveloped considering the region's relevance to the People Republic of China's sustenance and socio-economic development. Identifying and establishing causal relationships is vital to interpreting how a cause or a combination of factors influences an outcome. Understanding these dynamics

The image pre-processing, processing, and map composition were conducted using ArcGIS 10.8, ENVI 5.0, and ENVI 5.3. Additional image pre-processing procedures (Fig. 2) included image calibration, layer stacking, and supervised classification. The types of imagery used for analysis were obtained from the LANDSAT 4 TM, LANDSAT 5 TM, LANDSAT 7 ETM+ datasets (using spectral bands 7, 4, and 2 together), and the LANDSAT 8 OLI/TIRS dataset (using spectral bands 7, 5, and 3 together). The satellite data corresponds to paths/rows 123, 124/035, 036, and 037.

Change Detection Analysis

Change detection analysis was run to ascertain the regularity of land use systems and its driving mechanisms in Henan Province, using Eqns. 1–3:

$$\text{Change in LULC} = \frac{LULC_{\text{Current year}} - LULC_{\text{Past year}}}{LULC_{\text{Past year}}} \dots \quad (1)$$

$$\% \text{ Change in LULC} = \frac{LULC_{\text{Current year}} - LULC_{\text{Past year}}}{LULC_{\text{Past year}}} \times 100\% \dots \quad (2)$$

$$\text{Rate of change in LULC per year} = \left[\left(\frac{LULC_{\text{Current year}} - LULC_{\text{Past year}}}{LULC_{\text{Past year}}} \right) \times 100\% \right] \div N \text{ years} \dots \quad (3)$$

where:

$LULC_{\text{Current year}}$ – the final year under study (2023) within the context of the present study,

$LULC_{\text{Past year}}$ – the initial year being studied (1983),

N – the difference in the understudied year span, thus, 40 years.

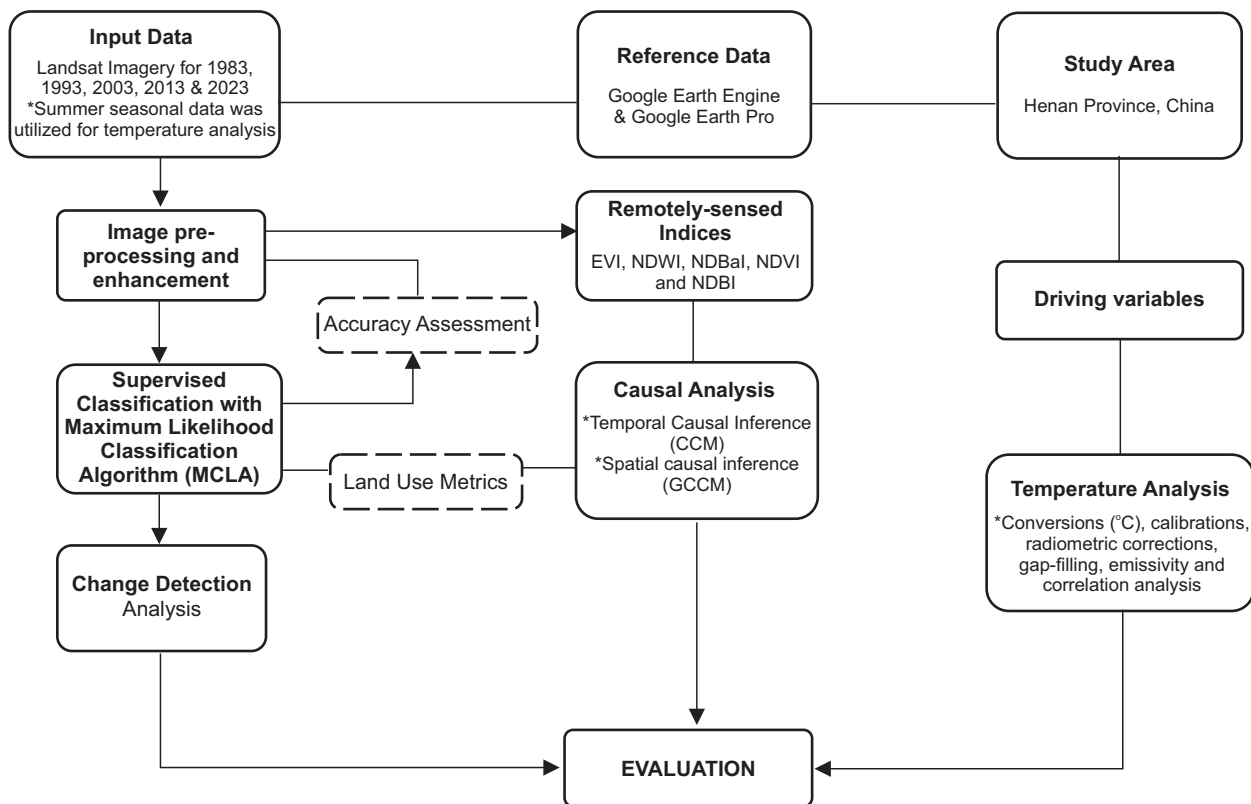


Fig. 2. Workflow for image preprocessing and post-classification designed for the study (source: Authors' own elaboration)

The rate of change in LULC per year was computed to ascertain the gains/expansion and losses/reduction in areas covered by the given land use classes (refer to Table A.1) over the past 40 years. This provides detailed information on how changes occurred annually to substantiate major events, transitions and underlying mechanisms that drove such changes. The expressions used in computing landscape metrics are captured in the supplementary material (See appendix).

Temperature analysis

Radiometric correction (radiance) was applied to rectify atmospheric effects and enhance clarity. Gap-filling was performed for images that may have had stripes. Distortions in images were removed in the calibration process to enhance image quality. We tailored the conversion of DN to spectral radiance according to the procedures of Coll et al. (2010), as retrieved from USGS Landsat User handbook. The ETM + DN values range between 0 and 255. Equation (4) was used to determine the radiance for the study domain:

$$L_{\lambda} = \frac{(LMAX_{\lambda} - LMIN_{\lambda})}{(QCALMAX - QCALMIN)} \times (DN - QCALMIN) + LMIN_{\lambda} \dots \quad (4)$$

where:

L_{λ} – cell value, simplified as radiance in $\frac{w}{(M^2 \cdot sr \cdot \mu m)}$,

$LMAX_{\lambda}$ – sensor spectral radiance scaled to ($QCALMAX$) in $\frac{w}{(M^2 \cdot sr \cdot \mu m)}$,

$LMIN_{\lambda}$ – sensor spectral radiance scaled to ($QCALMIN$) in $\left[\frac{w}{(M^2 \cdot sr \cdot \mu m)} \right]$,

($QCALMAX$) – maximum quantized calibrated pixel value that corresponds to $LMAX_{\lambda}$ [DN],

($QCALMIN$) – minimum quantized calibrated pixel value corresponding to $LMIN_{\lambda}$ [DN],

$QCAL$ – quantized calibrated pixel value [DN].

$LMIN$ and $LMAX$ – spectral radiances for each band at DN 1 and 255 for Landsat 7 ETM+ 1 and 65535 for Landsat 8 OLI/TIRS,

λ – the wavelength.

Conversion of Spectral Radiance (L_{λ}) to Kelvin with emissivity value (Eqns. 5–6) is conducted as follows:

$$T = \frac{K_2}{\ln \left(\frac{K_1 \cdot E}{L_{\lambda}} + 1 \right)} \dots \quad (5)$$

$$BT = \frac{K_2}{\ln \left[(K_1 / L_{\lambda}) + 1 \right]} \dots \quad (6)$$

Table A.2 presents k_1 and k_2 becoming coefficients, determined by effective wavelength of a satellite sensor based on these constants. Removal of atmospheric distortions from the thermal infrared data was performed using ENVI 5.0 software for the correction of thermal band 10 (Table A.3). Values generated were converted from Kelvin (K) (T_B) to degree Celsius ($^{\circ}C$) using the expression (eqn.7). It is worth noting that only summer seasonal data was used in the analysis.

$$T_C = T_B - 273.15 \dots \quad (7)$$

Indirect causality analysis: Temporal and spatial causal relationship between LULCC and LST

In this study, we focus on Henan Province to explore the temporal and spatial indirect causal relationship between LULCC variables and land surface temperature (LST). In the dynamic urbanization context of Henan, characterized by extensive urban expansion and industrial growth, we sought to understand how specific LULCC variables influence the development and intensification of LST. Through the analysis of satellite imagery, temperature data, and Henan-specific land use data spanning recent decades, Geographical Convergent Cross Mapping (GCCM) and Convergent Cross Mapping (CCM) causal analysis are employed to reveal spatial patterns and temporal trends. Using causal models (Gao et al., 2023), we sought to establish a causal link between LULCC variables and LST in Henan, considering unique contextual factors. The findings provide insights into the implications for urban planning and environmental management in Henan Province, contributing to a broader understanding of LULCC and LST dynamics in rapidly urbanizing regions. Future research recommendations could focus on the evolving urban landscape in Henan,

emphasizing the importance of sustainable urban development in this context. Expressions and variables used in computing temporal and spatial causal inferences are detailed in the supplementary material (see appendix).

Land use prediction and validation

Forecasts for 2033, 2043, and 2053 (Fig. 3) were created using the Modules for Land Use Change Evaluation (MOLUSCE) in QGIS software version 2.18.24. This plugin utilizes Cellular Automata and Artificial Neural Network (CA-ANN) techniques and simulations to make predictions for Henan Province. The analysis primarily involves Evaluating Correlation (EC), area changes, Transition Potential Computation (TPC) modeling, and validation based on four iterations. To make these predictions, a Digital Elevation Model (DEM) and a road raster georeferenced image of Henan Province were used as reference data. The key variables used as references for future projections

include the built environment (such as the likelihood of change, density of developed lands, crop land, and transportation), socio-economy (including population density, number of households, urban population density, urbanization, and industrialization), and natural environment (such as climatic variables - temperature, precipitation, and moisture, as well as ecological and topographical variables).

Accuracy Assessment

In examining the accuracy of each study period, ground truth sample points were obtained using ENVI 5.0 and ArcGIS 10.8 software. These points were overlaid on Google Earth Pro for verification. Hundred sample points were generated from each class in the classified images for accuracy assessment (Fig. 4). We employed Congalton (1991) confusion matrices, cited in Sarfo et al. (2022) (equation 8) to validate the spatial results obtained for this study. This standardized matrix (https://pages.cms.huberlin.de/EOL/geo_rs/S10_

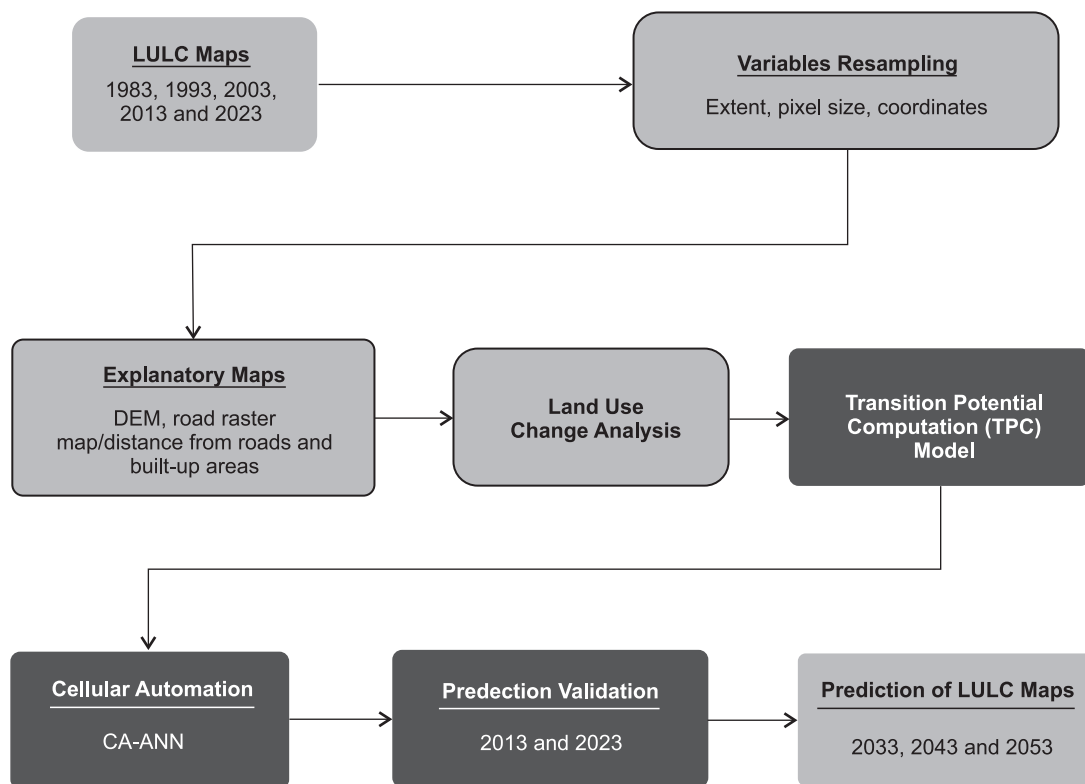


Fig. 3. Evaluation of land use predictions procedures (source: Authors' own elaboration)

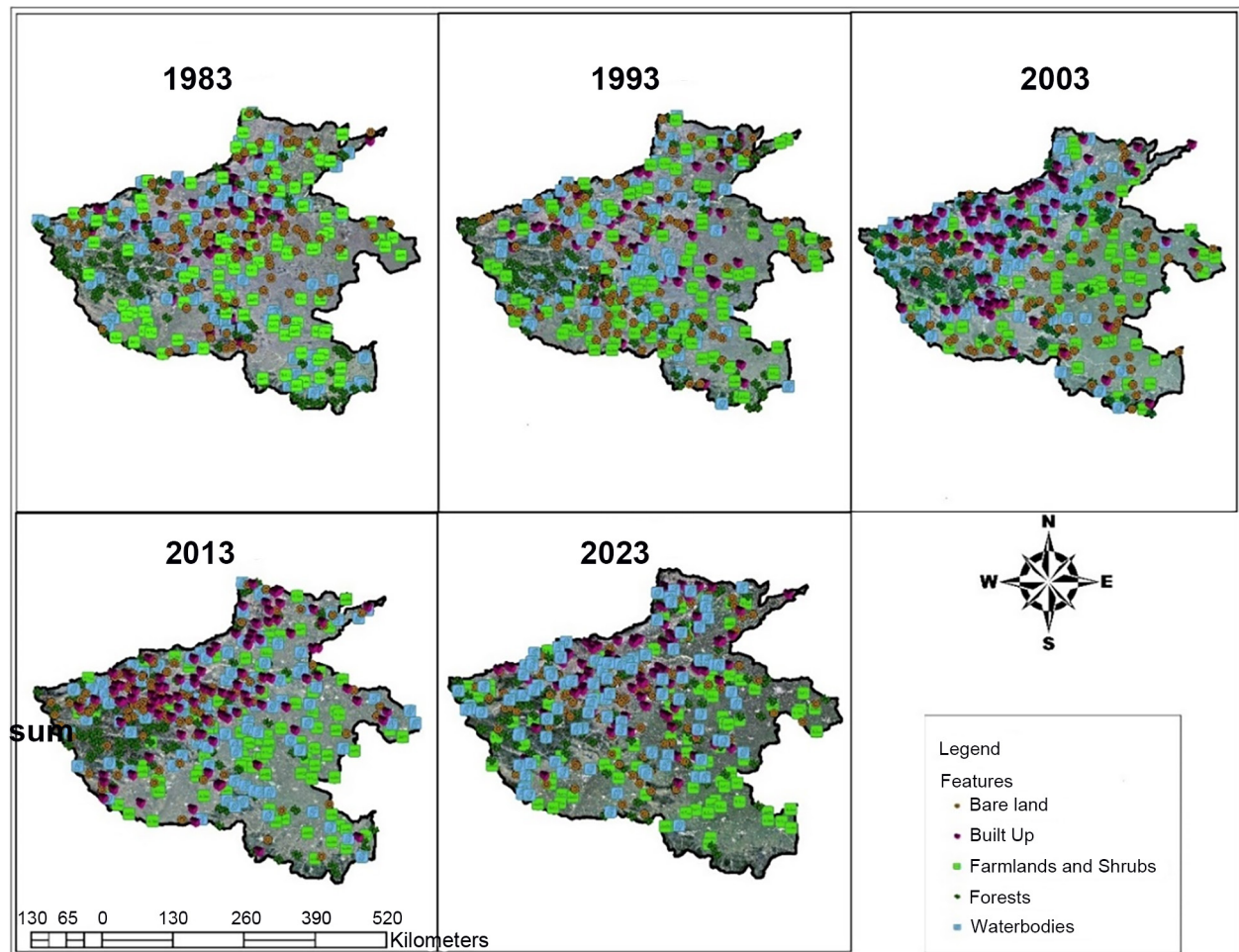


Fig. 4. Accuracy assessment of satellite imagery over the given study period (source: Authors' own elaboration)

Accuracy_assessment.html#Confusion_matrix) combines and improves upon the user and producer accuracy assessments applied by several scholars and research institutes across the globe to ensure validity and accuracy in images generated.

$$\text{Accuracy Assessment (AA)} = \left[\left(\frac{ASP}{TSP} \right) \times 100 \dots \right] \quad (8)$$

where:

ASP – number of sample points that accurately fall on each required feature (*ASP* = 450),

TSP – number of total sample points generated (*TSP* = 500),

AA = Accuracy Assessment $\left[\left(\frac{450}{500} \right) \times 100 = 90\% \right]$.

Therefore, the present study had 90% accuracy over the study period considering the samples collected.

RESULTS

Spatial distribution of Henan Province's land use systems

The given distributions (Tables 3, 4 and 5) indicate land cover conversion over the past 40 years for each land cover type. Fig. 5 shows that built-up areas (+500.46%), forests (+50.88%) and water bodies (+83.56%) were the key land cover types, which expanded massively between 1983 and 2023. By contrast, a reduction can be observed for farmlands/shrubs (–20.81%) and bare land (–60.53%) over the same period.

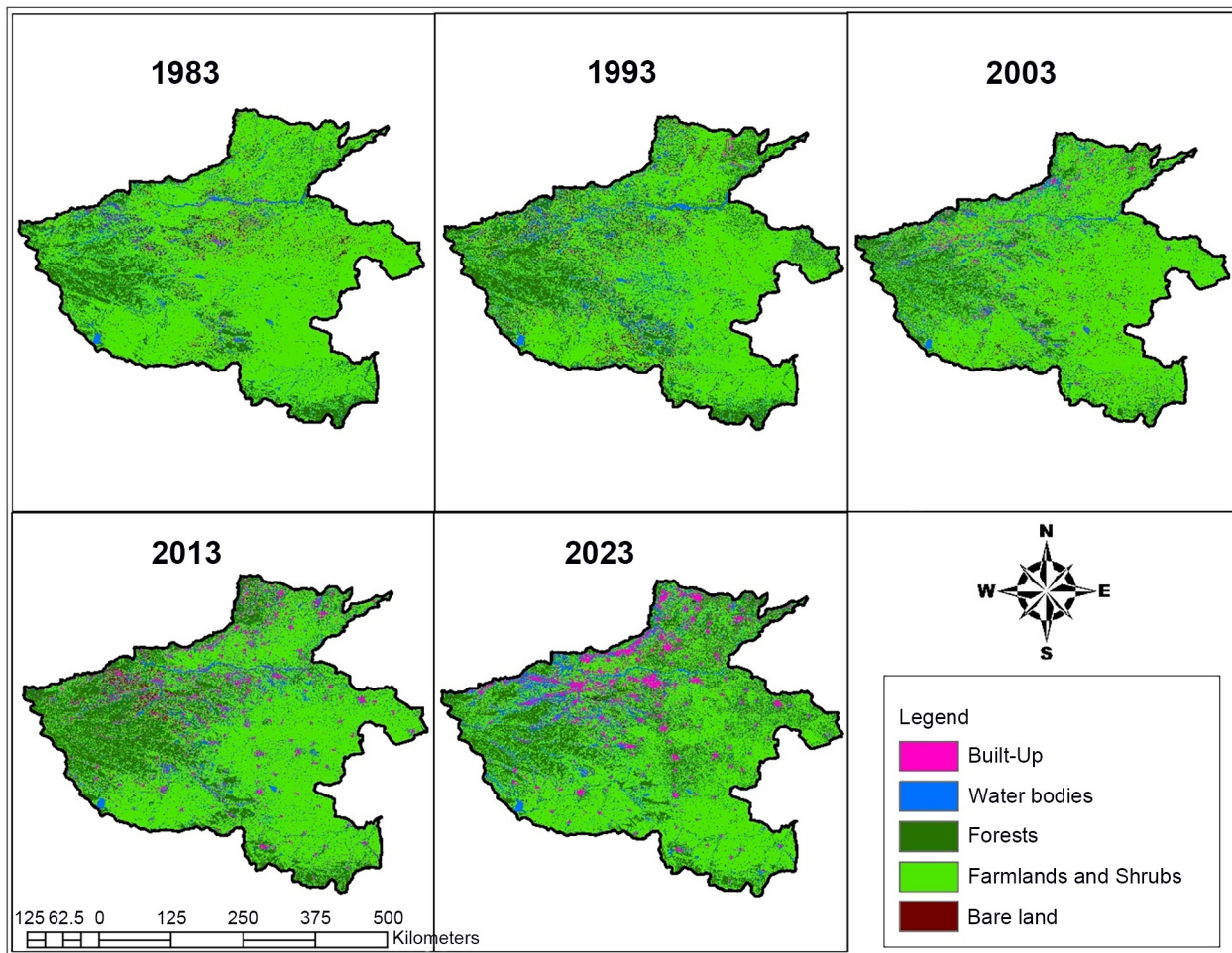


Fig. 5. Henan Province’s land use cover changes between 1983 and 2023 (source: Authors’ own elaboration)

Table 3. Area coverage for each class (km²) in Henan Province (1983–2023) (source: Authors’ own elaboration)

Class/Period	1983	1993	2003	2013	2023
Farmlands/ shrubs	12 6032	113 186	123 175	104 785	99 808
Bare land	5 419	8 377	4 588	3 038	2 139
Built-up areas	1 723	1 799	3 905	8 269	10 432
Forests	22 858	27 245	20 865	33 729	34 488
Water bodies	10 968	16 393	14 467	17 179	20 133

***Total area coverage (km²) (Absolute) = 167.000

Table 4. Temporal variations of land cover changes (LCC) (%) for Henan Province (1983–2023) (source: Authors’ own elaboration)

Class/Period	1983–1993	1993–2003	2003–2013	2013–2023	1983–2023
Farmlands/shrubs	–10.19	+8.83	–14.93	–4.75	–20.81
Bare land	+54.59	–45.23	–33.78	–29.59	–60.53
Built-up areas	+4.41	+117.07	+111.75	+26.16	+500.46
Forests	+19.19	–23.42	+61.65	+2.26	+50.88
Water bodies	+49.46	–11.75	+18.75	+17.19	+83.56

Table 5. Rate and magnitude of change (sq.km) of LCC in Henan Province (source: Authors’ own elaboration)

Class/Period	1983–2023				
	1983	2023	Magnitude of Δ (km ²)	Rate of Δ /Yr (%)	Magnitude of Δ (km ²)/Yr
Farmlands/shrubs	126 032	99 808	–26 224	–0.5	–655.6
Bare land	5 419	2 139	–3 280	–1.5	–82
Built-up areas	1 723	10 432	+8 709	+12.5	+217.7
Forests	22 858	34 488	+11 630	+1.3	+290.75
Water bodies	10 968	20 133	+9 165	+2.1	+229.1

Land Surface Temperature (LST) evaluation

A fundamental drift in LST can be observed throughout the study period. Seasonal droughts in China have long prevailed over China, particularly over the past few decades. For emphasis, temperature variations reported in this study for Henan Province utilized seasonal summer data due to the data acquisition date that presents an appropriate mean maximum and minimum temperatures for further analysis. Fig. 6 shows mean maximum (33.7°C) and minimum (20.9°C) temperatures during summer over the last 40 years. Overall, the annual average temperature for the study domain is 15.6°C.

Evaluation of remotely-sensed indices for Henan Province

Enhanced Vegetative Index (EVI)

Fig. 7 presents spatiotemporal dynamics of vegetation health and density across Henan Province between 1983 and 2023. Observations from the spatial analysis identify areas with dark green patches as high EVI hotspots, whilst light green, yellowish and dark brown zones mark areas with moderate to low EVI spots. A close observation shows how most EVI hotspot zones within the far western, eastern, and southernmost parts of Henan Province like Xinyang, Yongcheng, Zhoukou, Shuizhai, etc. have several water bodies, mainly rivers, in their catchments. Additionally, it is worth noting that most parts of western Henan, with dark green areas are characterized by elevation or high altitudes with dense

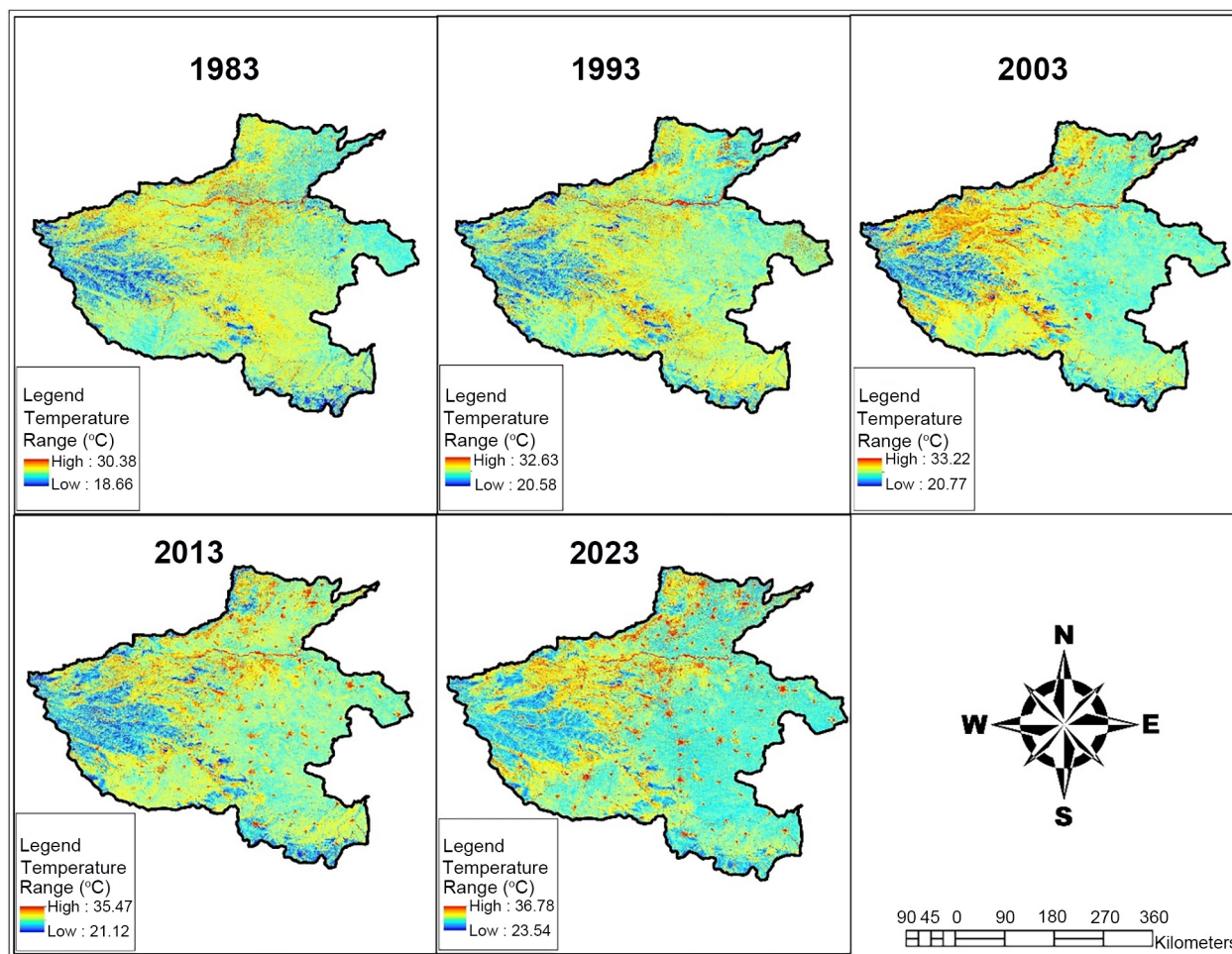


Fig. 6. LST variations for Henan Province during summer (1983–2023) (source: Authors' own elaboration)

vegetation coverage. Other areas displayed stable or fluctuating EVI trends concurrently, suggesting a complex interplay of various factors such as land use changes driven by economic impulses that move beyond population growth, such as urbanization and industrialization, among other rural revitalization strategies, as well as climate-induced and conservation parameters. A close observation shows a mix of EVI patterns, coinciding with rapid urban sprawl and infrastructural development during the 1993–2003 period. The 2003–2013 and 2013–2023 regimes reflected complex vegetation transitions in response to urbanization, industrialization and ecological civilization initiatives.

Normalized Difference Built-Up Index (NDBI)

Assessment of NDBI (Fig. 8) in the area revealed significant fluctuations of built environment/settlements and urbanization trends. The generated NDBI values (Fig. 8) demonstrated spatial variability across the province, reflecting the varying degrees of urban expansion and LUC. NDBI slowed down between 1983 and 1993 due to prolonged dryness, droughts and famine that occurred between the 1980s and 1990s across the globe. This propelled a shift in other land use forms like farmlands/shrubs and migration in subsequent windows; thus, in the 1993–2003 period. This corresponds to rural development in subsequent periods, and spatial trends observed in Figs. S1–S2. A considerable increase in NDBI for 1993–2003 and

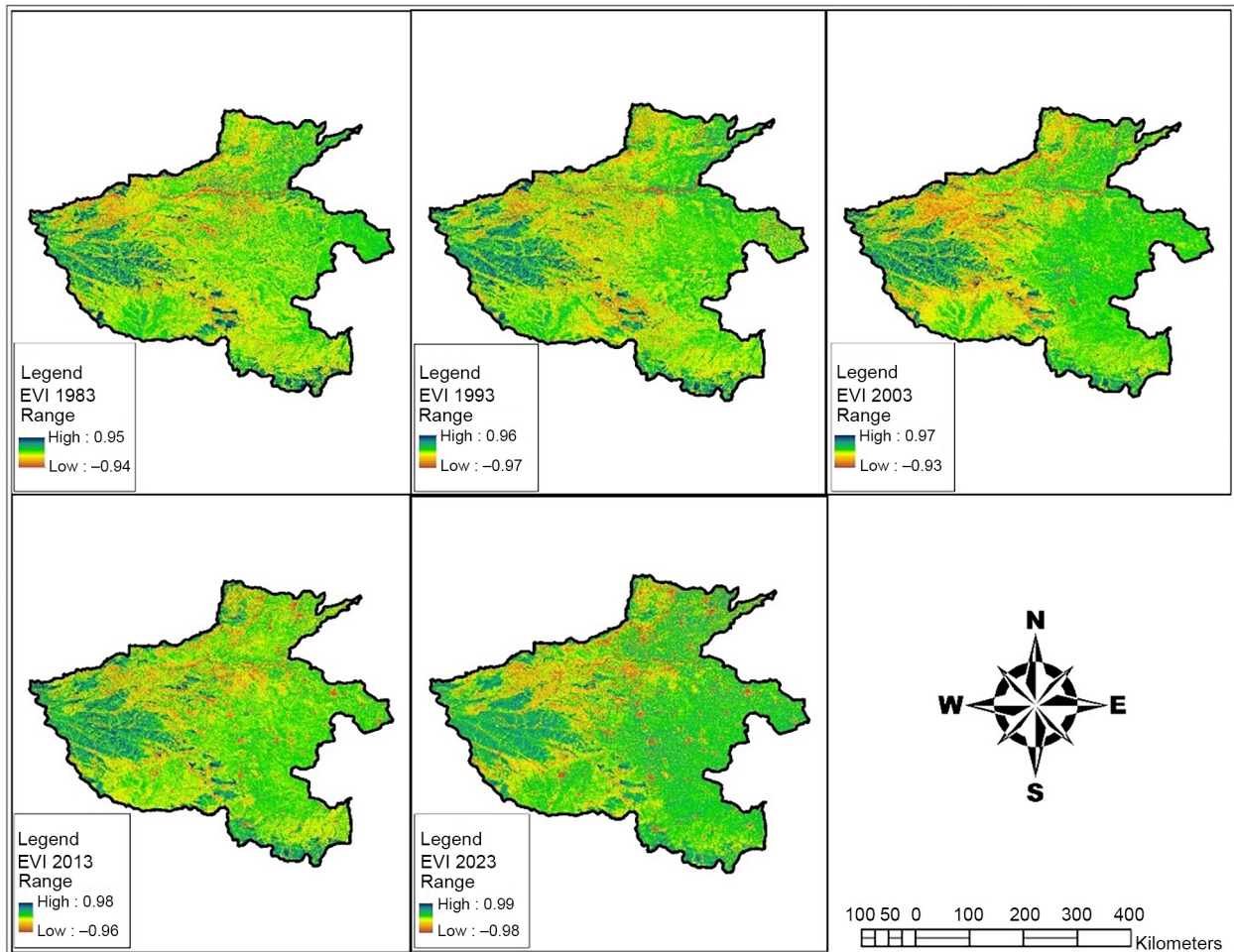


Fig. 7. EVI variations in Henan Province (1983–2023) (source: Authors’ own elaboration)

subsequent decades affirm evidence of urbanization, economic growth and infrastructure expansion, driven by an array of policy-driven factors. Dark red zones mark areas with high urban concentration (i.e., cities and urban areas) like Zhengzhou, Shangqiu, Luoyang, Nanyang, Xinyang, Xinxiang, Hebi, Jia-zuo, Anyang, etc. Areas with yellow, cyan, green and magenta color patches mark zones with moderate built environment to areas with low built-up concentration (i.e., sub-urban, rural and areas covered by water bodies).

Normalized Difference Water Index (NDWI)

Fig. 9 illustrates that areas covered by water bodies have undergone expansion. Dark blue areas exhibit

areas with high NDWI, whereas green to light yellow/green zones indicate areas with moderate or low NDWI. Continuous and recurrent changes in NDWI can be observed across Henan Province. NDWI is high around Huanglongsi, Kaifeng, Luoyang, Jiyuan, Zhumadian, Nanyang and its environs, due to the presence of major rivers as illustrated in the study area map (Fig. 1). A steady increase was observed between 1983 and 2003 due to extreme climatic conditions experienced around the globe. However, NDWI plummeted between 2003 and 2023 due to the unprecedented heavy rains and historical flooding event that occurred in Zhengzhou (i.e., the provincial capital) and across Henan province between July 17 and 31 2021. This historical event had dire

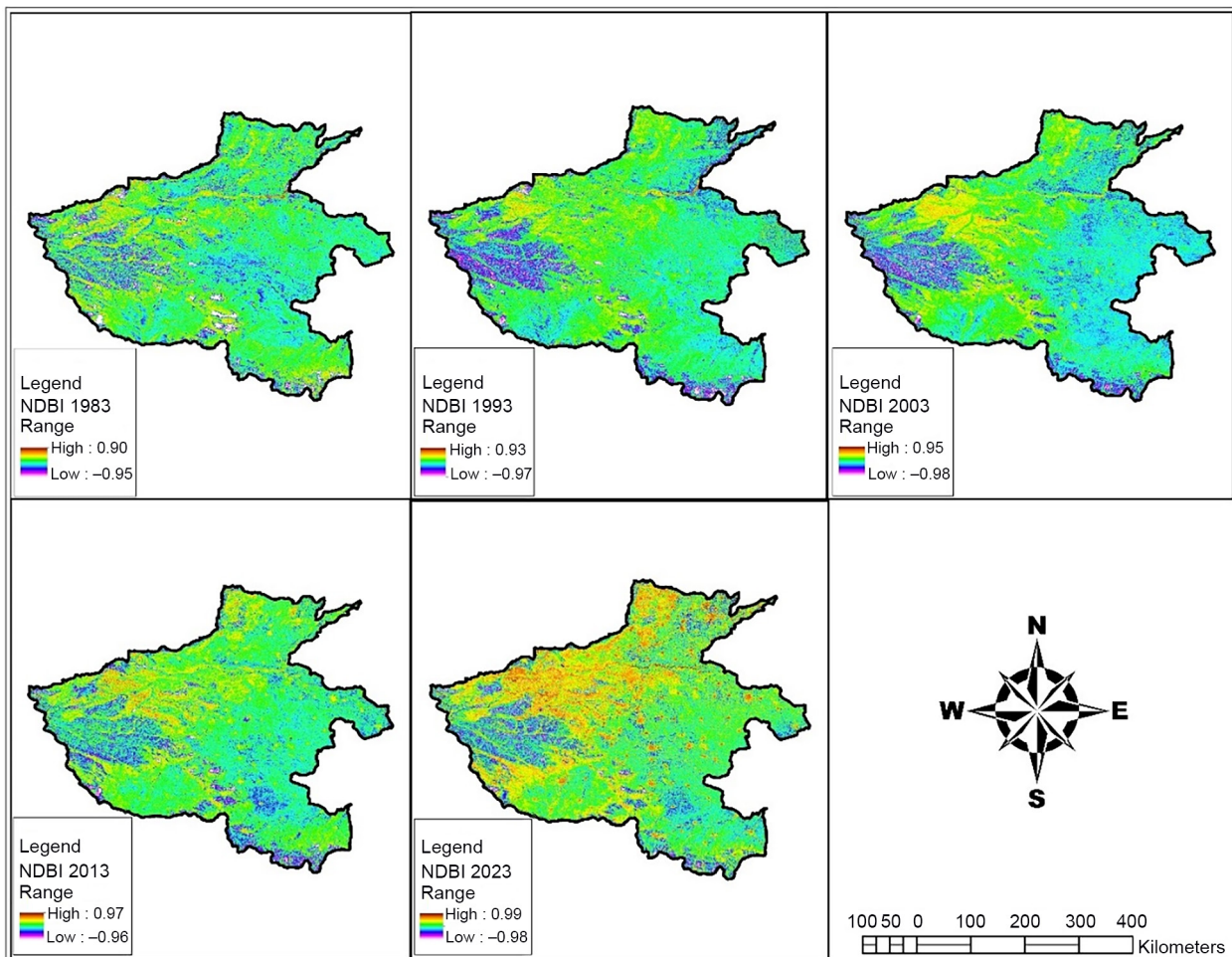


Fig. 8. NDBI variations in Henan Province (1983–2023) (source: Authors’ own elaboration)

consequences by inundating hundreds of villages, claiming lives and driving several economic losses worth billions. Early studies (Chen et al., 2022; Hsu et al., 2023) had reported human driven climate-induced factors amplified the rain that fell. Expansion in Henan Province’s water bodies can be attributed to climate-induced stressors such as temperature rise, resulting in the expansion of water bodies and expansion of irrigational projects, aimed to enhance industrialization, granary and agricultural productivity in the region. Again, regrowth in forested areas serves as cover for water bodies, hence, somewhat influencing these expansions.

Normalized Difference Bareness Index (NDBaI)

Fig. 10 provides insights into changes in barren areas or impervious surfaces within the province in Central China. NDBaI (Fig. 10) exhibited spatial heterogeneity across the province, reflecting varying degrees of bareness/imperviousness in different areas. A general decline in barren areas based on spatial analysis presented in Fig. 5 indicates bare land has been replaced by the natural vegetation through ecological restoration/greener landscapes, and by built-up areas between 1983 and 2023. The continuous variations in NDBaI are in tandem with urbanization trends (Figs. S1–S2). Fig. S1 depicts areas with white and dark brown patches, indicating high NDBaI. Similarly, areas with high altitudes in the western part of

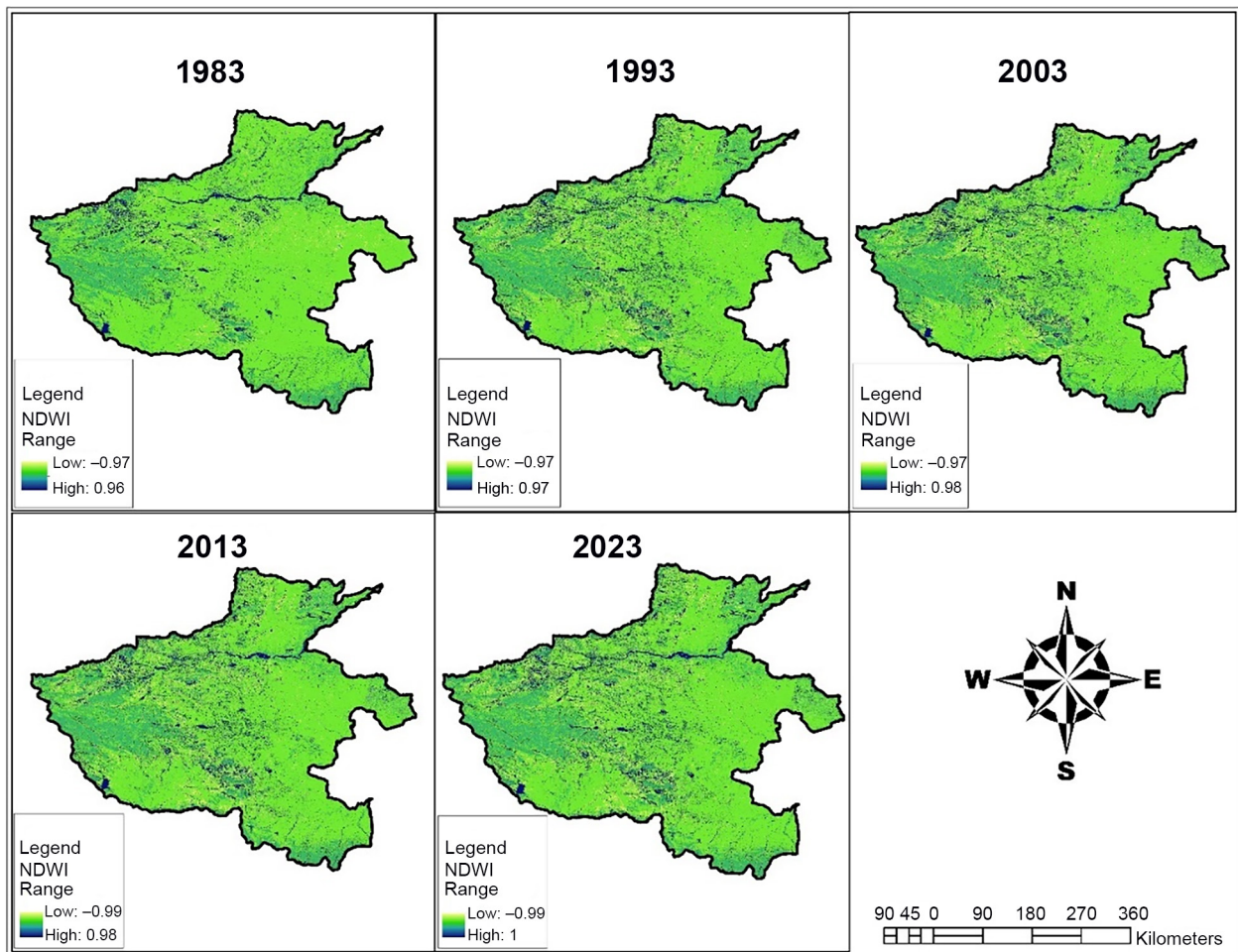


Fig. 9. NDWI variations in Henan Province (1983–2023) (source: Authors' own elaboration)

Henan Province can be observed, particularly those marked by dark brown spots. Barren areas are being cleared for farming or construction purposes around water bodies, in and around cities such as Nanyang, Huazhou, Xinyang, Jiyuan, Pingdingshan, and their surrounding areas. On the other hand, domains with low barren surfaces are indicated by green and light brown spots.

Temporal causal inference

The patterns depicted in Figure 11 reveal a strong indirect convergence (Fig. 11a–b) between built-up areas and LST, underscoring built-up areas' profound impact on LST intensity/patterns. A moderate indirect

convergence is evident (Fig. 11c–d) between bare land and LST, signifying the moderate influence of bare land on LST. While an indirect convergence is observed in terms of the impact of water bodies on LST, the extent of their significant influence on LST intensity in Henan Province remains unclear, as illustrated in Fig. 11e. Notably, there is substantial indirect convergence (Fig. 11f) between forest and LST, highlighting the dominant effect of forests on LST. Furthermore, a strong indirect convergence (Fig. 11g) is observed between farmlands/shrubs, and LST, indicating that farmlands/shrubs play a regulatory role in influencing LST.

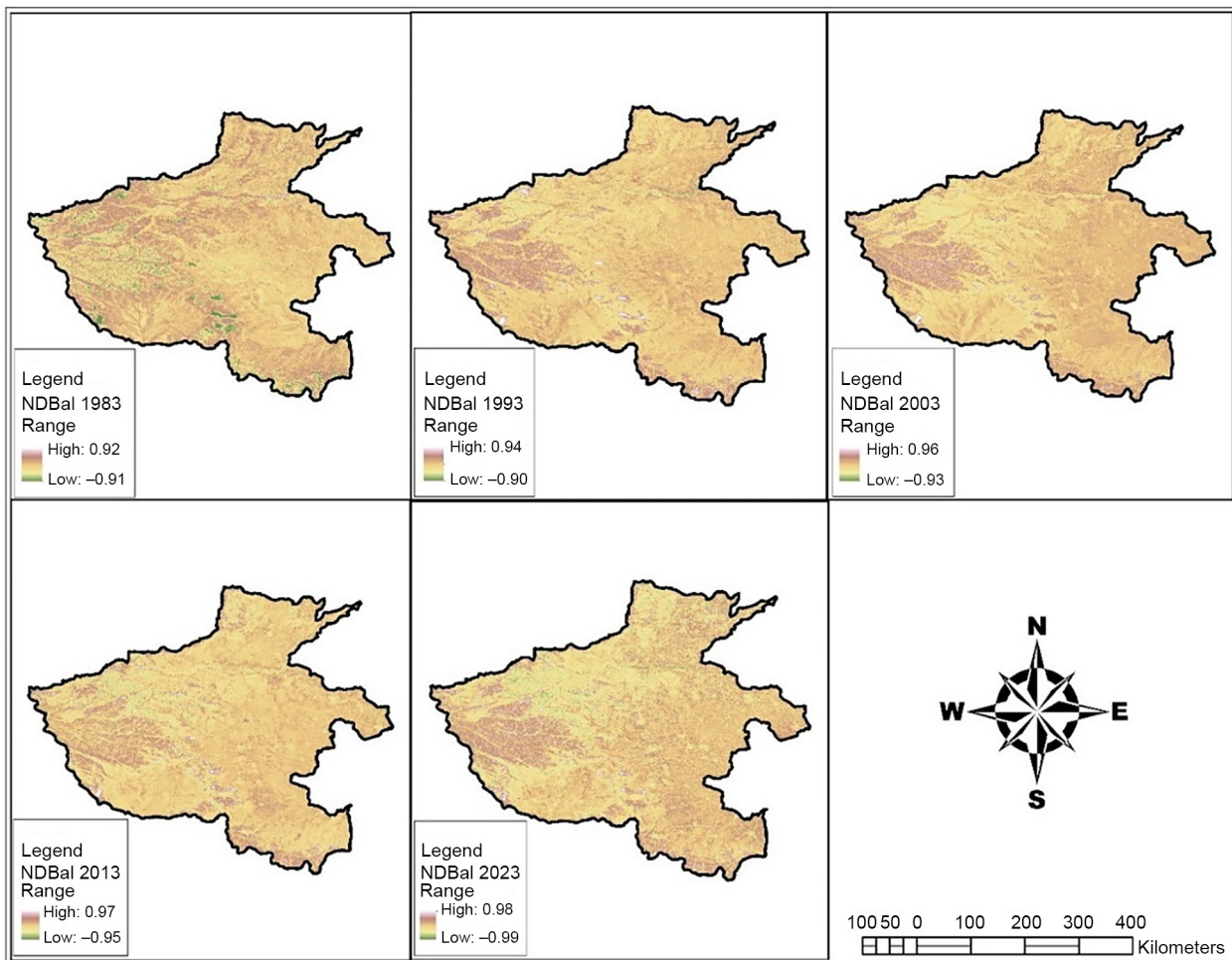


Fig. 10. NDBal variations in Henan Province (1983–2023) (source: Authors' own elaboration)

Spatial causal inference

In Fig. 12 (a, b), a positive cross-mapping skill value ($\rho = 0.63$) indicates a robust positive indirect cross-mapping relationship between built-up areas and LST. This implies that the presence or attributes of built-up areas can be utilized to predict or elucidate the patterns of LST to a considerable extent. Furthermore, a positive value ($\rho = 0.32$) in Fig. 12 (a, c) signifies a moderate positive indirect cross-mapping relationship between bare land and LST. This suggests a moderate positive association between the characteristics of bare land and the LST phenomenon.

Nevertheless, a negative cross-mapping skill value ($\rho = -0.36$) indicates a moderate negative indirect cross-mapping relationship in Fig. 12 (a, d) between areas covered by water bodies and LST. This sug-

gests that areas covered by water bodies might have a cooling effect on LST, contributing to lower LST values. Additionally, a negative value of ($\rho = -0.12$) in Fig. 12 (a, e) indicates a negative indirect cross-mapping relationship between forest and LST. This implies that areas covered by forests might have a cooling effect on LST, contributing to lower LST values. It is worth noting that different types of vegetation have varying degree or cooling effects on LST. Furthermore, a negative value of ($\rho = -0.27$) in Fig. 12 (a, f) suggests a relatively moderate negative indirect cross-mapping relationship between farmlands/shrubs and LST. This implies that LST patterns are inversely related to the characteristics of farmlands, and farmlands might contribute to lowering LST intensity in the area.

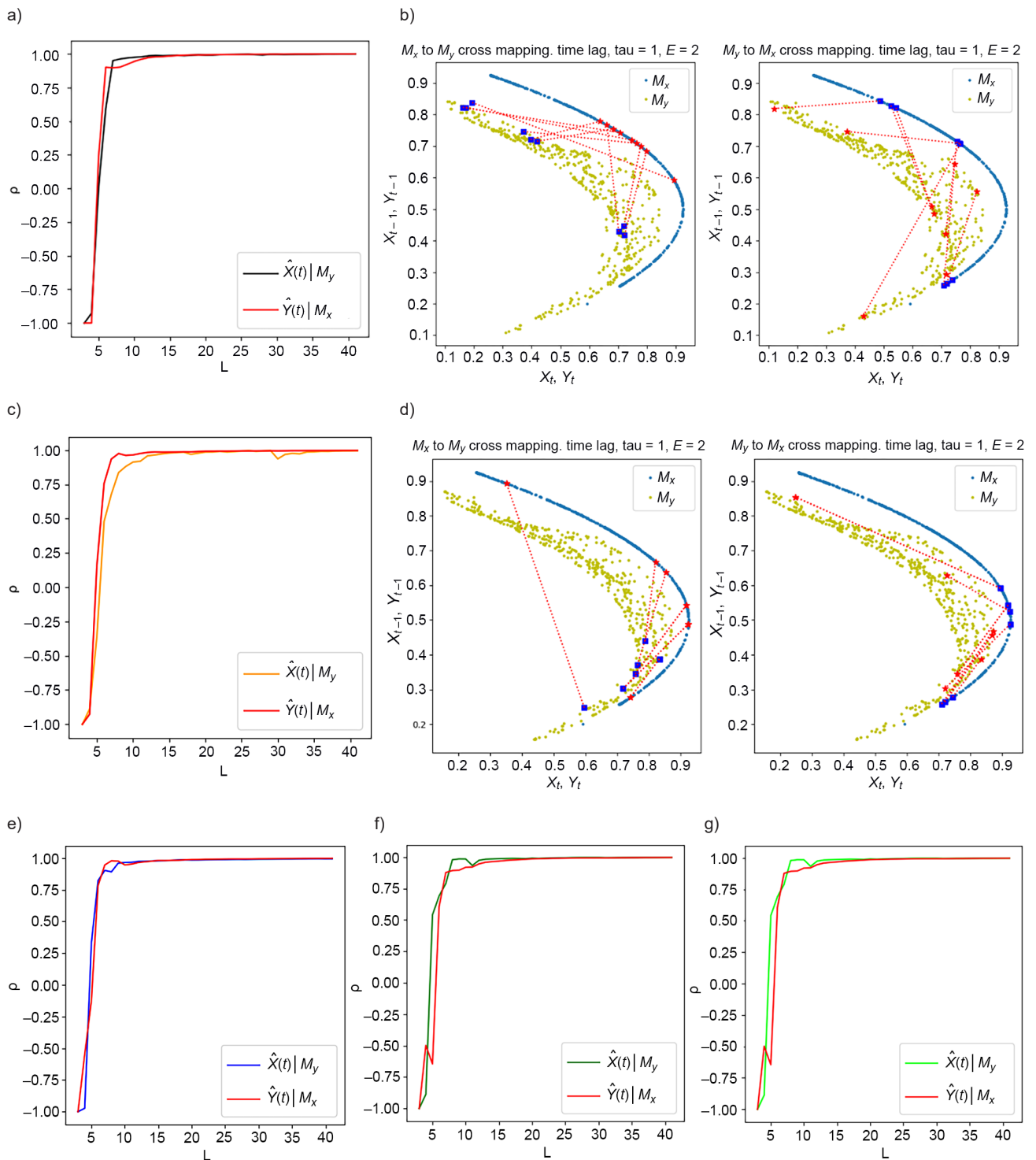


Fig. 11. Temporal causal inference of LULCC variable and LST: Built Up -LST causality and xmap (a, b); Bare land-LST causality and xmap (c, d); Water bodies-LST causality (e); forest-LST causality (f) and Farmlands and Shrubs-LST causality (g) (source: Authors' own elaboration)

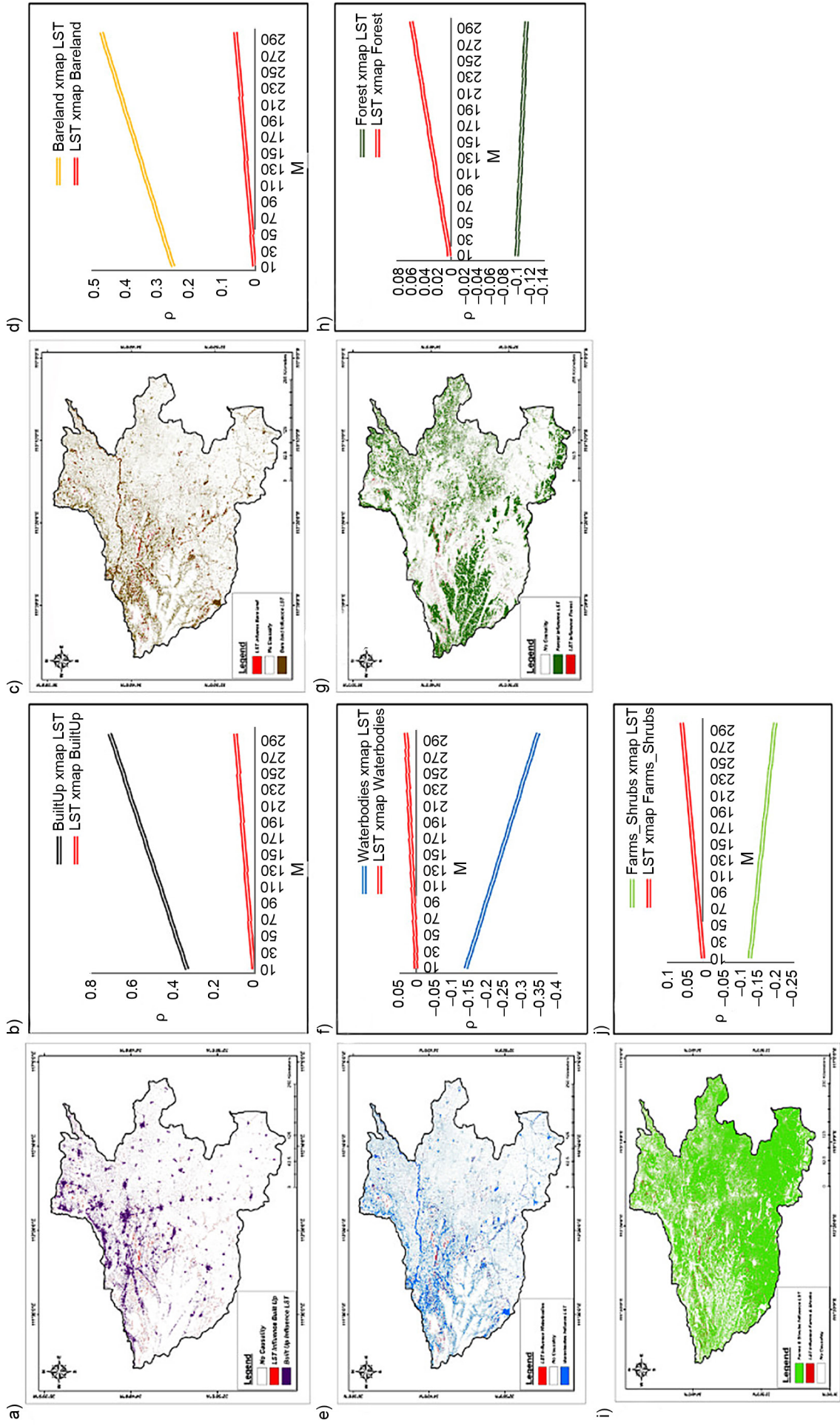


Fig. 12. Spatial causal inference of LULCC variable and LST: Built Up-LST causality and xmap (a, b); Bare land-LST causality and xmap (c, d); Water bodies-LST causality (e, f); forest-LST causality (g, h) and Farmlands and shrubs-LST causality (i, j) (source: Authors' own elaboration)

Land-use predictions for Henan Province (2033–2053)

The simulations (Fig. 13 and Table 6) show built-up and farmlands/shrubs will expand at a rate of 117.3% (with 3.9% increment annually) and 10.7% (with 0.4% annual expansion), respectively, over the next three

decades. Conversely, forests, barren and areas covered by water bodies will undergo a steady decline by 61.6% (at a 2.1% reduction rate each year), 39.7% (at a 1.3 decreasing rate annually) and 4.2% (at a 0.1% reduction rate annually), respectively, over the same period.

Table 6. Area coverage, temporal variations, rate and magnitude of change for each class in Henan Province (2023–2053) (source: Authors’ own elaboration)

Area Coverage for each class (sq. km) (2023–2053)				
Class/Period	2033	2043	2053	
Farmlands/shrubs	106,398	113,337	110,500	
Bare land	1,712	1,471	1,290	
Built-up areas	13,226	18,829	22,671	
Forests	24,837	15,837	13,252	
Water bodies	20,827	17,526	19,287	

Temporal variations				
Class/Period	2023–2033	2033–2043	2043–2053	2023–2053
Farmlands/shrubs	+6.6	+6.5	–2.5	+10.7
Bare land	–19.9	–14.1	–12.3	–39.7
Built-up areas	+26.8	+42.4	+20.4	+117.3
Forests	–27.9	–36.2	–16.3	–61.6
Water bodies	+3.5	–15.9	–10.1	–4.2

Rate and magnitude of change					
Class/Period	2023	2053	2023–2053		
			Magnitude of Δ (km ²)	Magnitude of Δ (km ²)/yr	Rate of Δ /yr (%)
Farmlands/shrubs	99808	110,500	+10,692	+356.4	+0.4
Bare land	2139	1,290	–849	–28.3	–1.3
Built-up areas	10432	22,671	+12239	+407.9	+3.9
Forests	34488	13,252	–21236	–707.9	–2.1
Water bodies	20133	19,287	–846	–28.2	–0.1

***Total area coverage (km²) (Absolute) = 167,000

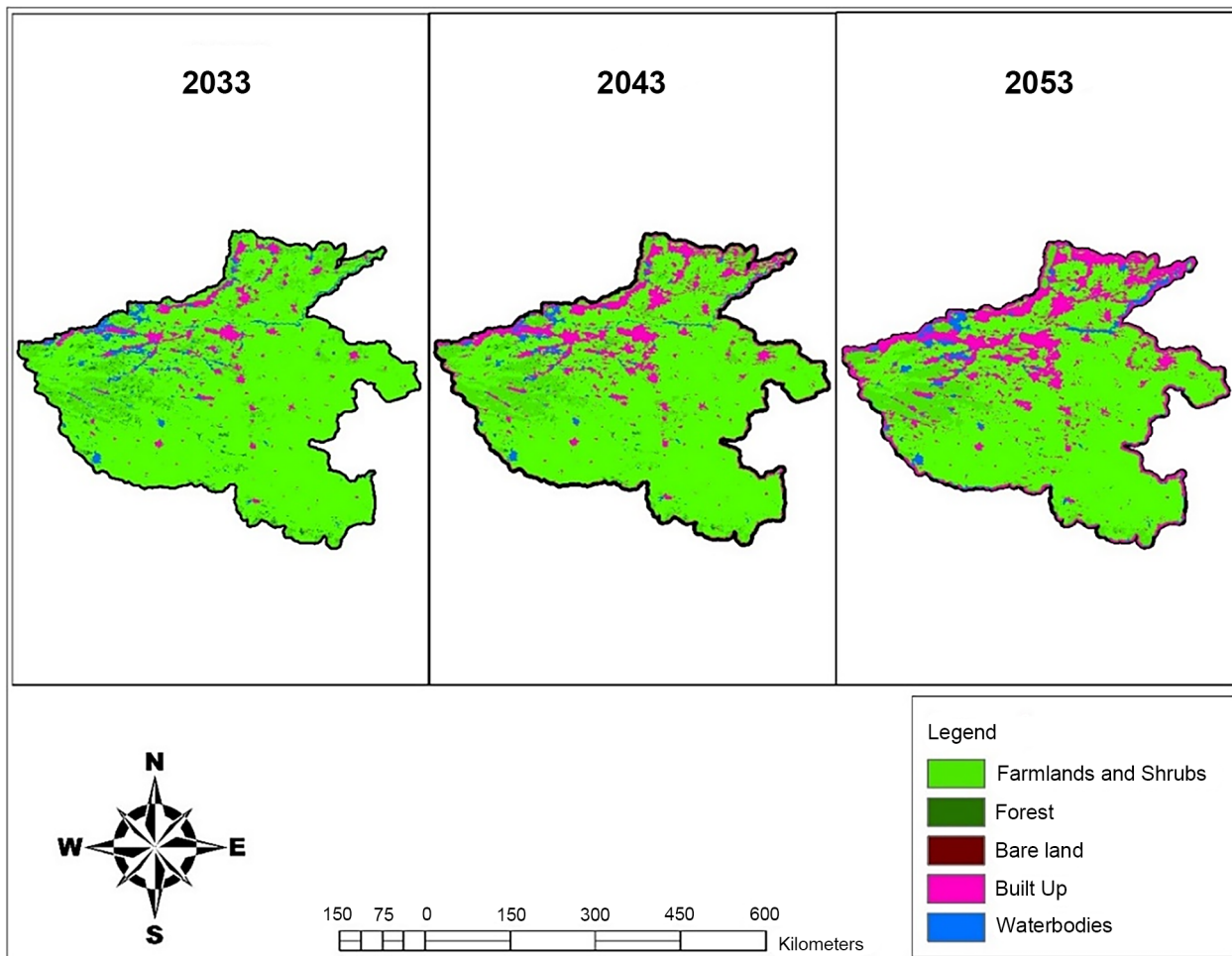


Fig. 13. Land-use predictions for Henan Province over the next three decades (2033–2053) (source: Authors' own elaboration)

DISCUSSION

Spatial distribution of land use systems in Henan Province

Scientific studies have extensively explored land use systems and climate variability within the context of sustainable development goals (SDGs) such as 11, 13, and 15. However, there is a relative scarcity of studies that thoroughly examine the interplay between remotely-sensed indices, policy-driven options, and causal analysis over long periods at the provincial or regional level. This is particularly true for Henan Province in Central China, which is characterized by ecological livability, rich cultural heritage, rural civ-

ilization, industrial prosperity, and immense agricultural productivity. Between 1983 and 2023, land use transitions in Henan Province, as shown in Table 4, reveal a gradual decline in farmlands/shrubs at an annual rate of 0.5%. Similarly, barren areas have experienced a decline of 1.5% over the past four decades. On the other hand, built-up areas, forests, and water bodies have expanded significantly during the same period, with annual growth rates of 12.5%, 1.3%, and 2.1%, respectively. While farmlands/shrubs were the dominant land use class in 1983, followed by forests and water bodies, there has been a fundamental shift in recent years. The expansion of built-up areas has been particularly exponential, despite being the least dom-

inant class in 1983. In the following sections, we will comprehensively evaluate land metrics and remotely-sensed indices, as well as the driving mechanisms behind these changes. We will also review relevant literature to support our findings.

Driving mechanisms of LULCC and LST based on causality analysis and relevant literature

Based on the results presented in sections 3.1 and 3.5, it is clear that Henan Province's land use and land cover is influenced by a combination of factors, including socio-cultural, political, economic, and environmental factors. While there was some convergence between the studied variables of LULCC and LST based on the results of the temporal causal inference analysis, it was found that built-up areas have the most significant impact on the intensity of LST in Henan Province. The influence of other variables such as forests, farmlands/shrubs, and water bodies on LST intensity in the study area remains unclear, especially when compared to the impact of built-up areas, which amplify LST. It is important to note that the type of vegetation plays a critical role in either triggering cooling effects or minimizing the effects of LST. This finding is consistent with the research conducted by Jin et al. (2020), who investigated the effect of vegetation variation on surface air temperature. Similarly, Sarfo et al. (2022) found that unlike forests, farmlands/shrubs have a minimal influence on LST, which aligns with the findings of this study. The analysis of spatial causal inferences (Fig. 12 a–c) shows a moderate to strong positive cross-mapping relationship between bare land, built-up areas, and LST. This suggests that the characteristics of these land features can be used to understand surface temperature patterns to a large extent. On the other hand, weak to moderate inverse cross-mapping values were observed for water bodies, forests, farmlands/shrubs, and LST. Contextually, these features have some regulatory impact on LST patterns/intensity (Fig. 12 e–j), but it is minimal. Interestingly, a closer examination of Fig. 12 (i) reveals that in some cases, farmlands/shrubs contribute to LST, possibly due to the presence of built-up areas or settlements around cultivated lands.

Based on the existing literature and the results of land metrics and causality analysis, the changes in Henan Province's land use systems can be largely attributed to population growth/distribution and pol-

icy-driven options related to the socio-economic and ecological development of the area. Biophysical parameters such as climate stressors (e.g., flooding) and terrain/topographical factors have also played a role in influencing these unprecedented changes. Between 1983 and 1993, initiatives were undertaken as part of the People's Republic of China's 40-year economic reform and opening-up policy. For example, directives such as the "preferential regional development strategy in the 1980s," "the 1992 Hinterland City opening-up policy," and the "Launching of urban greening regulation" led to the conversion of cultivated lands into built-up areas, settlements, and ecological/green landscapes (Mu et al., 2016). This trade-off of cultivated lands for infrastructure and economic development, particularly in the western, eastern, and central parts of China compared to the northern and southern regions, was aimed at bridging regional development gaps. This, in turn, resulted in changes in microclimatic conditions and increased settlements due to migration and high fertility/growth rates. The period from 1993 to 2003 witnessed a rapid rate of urbanization and industrialization. This was largely driven by increasing support and planning policies from the national/central government. State-driven policies, such as the 1994 Basic Agricultural Land Protection Regulations, the 1998 Requisition-Compensation Balance of Arable Land Policy, the 1999 "Grain-to-Green" policy, the National Landscape Garden City Policy, and the 2003 Coordinated Regional Development, led to a reconfiguration of the urban-rural landscape based on the Central Government's "five-coordinated strategies." These policies resulted in diverse development strategies and infrastructure development, with a focus on rural road construction/improvement in line with the saying "If you want to get rich, build roads first." As a result, barren areas, forests, and some water bodies were transformed into built-up areas and irrigational farms (Camille, 2020).

In the post-2000 era, specifically from 2003 to 2013, various regional policies were implemented in the province. These policies include the "2006 Requisition-Compensation Balance of Arable Land Policy", "2012 Urban-Rural Integration and Ecological Civilization Initiative", "Central Plain Urban Agglomeration (CPUA) Development Planning (2006–2010)", "Zhengzhou-Kaifeng New Urban Area Develop-

ment”, and “Forest Eco-City Planning”. These policies had a positive impact on the social stratification, economic welfare, and overall Gross Domestic Product (GDP) of both rural and urban residents. Additionally, early studies conducted by Mu et al. (2016), Camille (2020), and Li et al. (2022) revealed that these initiatives significantly influenced and reshaped the ecological landscape and security patterns of the province. As a result of these strategies, settlements were transformed, spontaneous migration occurred, and land and other resources were redistributed, all in the context of rural development and land consolidation efforts. From 2013 to 2023, the focus shifted to the “2017 rural revitalization initiatives”, aimed at eradicating poverty among rural residents living below the absolute or extreme poverty line. During this period, emphasis was also placed on the “Rising of Central China”, the connectivity of suburban areas to major cities, and the planning of the “Inter-City Railway Network in the CPUA”. The Central Plain Economic Region (CPER), as described by Chen et al. (2022) and Hsu et al. (2023), played a vital role in the overall development of the province.

Future of Henan Province based on land use predictions (2023–2053)

The continuous expansion of the built environment and the changing trajectory of farmland and shrub cover types indicate a need for a comprehensive and actionable roadmap to ensure sustainable growth in all aspects of the province. The central government aims to promote equitable economic growth through urbanization, industrialization, and rural revitalization. However, without regulation, the current economic and policy-driven initiatives that prioritize land development over other gains could have devastating consequences for farmland and shrub-covered areas in the province, as shown in Figure 13 simulations. These findings support the claims made by Zhao et al. (2021) in their study on “China’s future food demand and its implications for trade and the environment.” Spatial analysis highlights the urgent need to regulate urbanization (Wang et al., 2021) and other economic trade-offs involving land and resources for infrastructure development, as this will have long-term impacts on agricultural productivity. Additionally, Wang et al. (2021) have projected

a steady increase in built-up areas by 2050, which in turn leads to a decline in pristine environments. These findings align with the current study’s predictions of expansion in built-up areas and the reduction in forests, water bodies, and bare land, as farmland and shrub cover increase.

CONCLUSIONS

We conducted a study in Henan Province using an indirect causality approach to explore the effects of different land use systems on land surface temperature (LST). This region, which is predominantly rural, plays a crucial role in China’s socio-economic and environmental development. Additionally, we predicted future land use patterns for the next three decades based on current trends. The key findings are summarized as follows:

1. Henan Province is currently undergoing significant changes in its land use systems. The areas occupied by farmlands and shrubs are experiencing a decline of 20.81%. These unprecedented changes are mainly driven by factors such as population growth and distribution, industrialization, and policy-driven options. They are also closely linked to the Central Government’s economic reform and opening-up policy, which has been in effect for the past 40 years.
2. Currently, there is a noticeable regrowth or greening happening, which can be attributed to spatial trends and policy directives like “The ecological civilization initiative” implemented by the Central Government, as well as regional and local authorities.
3. The analysis of temporal causal inference, specifically the causal analysis, revealed a robust association between built-up areas and surface temperature. This finding provides substantial evidence to support the influential role of built-up areas on the intensity of land surface temperature.
4. Results from the spatial causal inference analysis shows moderate to robust positive indirect cross-mapping relationships between built-up areas ($p = 0.63$) and bare land ($p = 0.32$) against LST. This implies that the characteristics of built-up and barren areas can be utilized to predict or elucidate LST patterns to a considerable extent

in Henan Province. Contrarily, weak to moderate negative indirect cross-mapping relationships were observed for forests ($\rho = -0.12$), farmlands/shrubs ($\rho = -0.27$) and water bodies ($\rho = -0.36$). This implies they somewhat play regulatory roles in reducing LST intensity in some areas. Interestingly, it is worth noting that different types of vegetation have varying degrees of influence on LST patterns/intensity.

5. Land use predictions over the next three decades show continuous expansion in built environment (+117.3%), a reversed trend in farmlands/shrubs (+10.7%) currently under decline. Forests (-61.6%), bare land (-39.7%) and areas covered by water bodies (-4.2%) are expected to reduce.

To this end, understanding these dynamics is essential for safeguarding and managing rural landscapes, and enhancing Henan Province's environmental and agricultural informatization. Causality and relevant literature analyses demonstrate that shifts in Henan's land use systems moves beyond identifying population growth and distribution, and urbanization as the sole driving mechanisms of Henan's land-use/environmental changes. Instead, a combination of factors is responsible for these shifts. Furthermore, findings will facilitate the understanding of forecasting future land use patterns, based on current trends to optimize resource utilization and the need to address institutional, economic and environmental impacts emanating from these undesired changes. In future studies, researchers can utilize emerging digital technologies, such as innovative machine and deep learning approaches, to develop early warning systems. These systems could further be used to comprehensively investigate the spatiotemporal dynamics of land use systems in both high and emerging economic nations. Additionally, further studies could assess the dynamics of land use among rural residents, particularly in the context of rural revitalization and sustainability concerns.

DECLARATION OF COMPETING INTEREST

The authors declare that they have no known competing financial interests or personal relationships that could have appeared to influence the work reported in this paper.

DATA AVAILABILITY

The data that backs up the study's conclusions is accessible with the appropriate link provided in the methodology section.

CODE AVAILABILITY

Codes used for this study will be made available upon reasonable request.

REFERENCES

- Ahmed, B., Zhu, X., Rahman, S., Choi, K. (2019). Simulating land cover changes and their impacts on land surface temperature in Dhaka, Bangladesh. *Remote Sensing*, 5 (11), 5969–5998. DOI: 10.3390/rs5115969
- Avdan, U., Jovanovska, G. (2016). Algorithm for automated mapping of land surface temperature using LANDSAT 8 satellite data. *Journal of Sensors*, 1–8. DOI: 10.1155/2016/1480307
- Al, A., Rahman, S., Faisal, A. (2020). Modelling future land use land cover changes and their impacts on land surface temperatures in Rajshahi, Bangladesh. *Remote Sensing Applications: Society and Environment*, 18, 100314. DOI: 10.1016/j.rsase.2020.100314
- Asgarian, A., Amiri, B.J., Sakieh, Y. (2014). Assessing the effect of green cover spatial patterns on urban land surface temperature using landscape metrics approach. *Urban Ecosyst*, 18, 209–222. DOI: 10.1007/s11252-014-0387-7
- Aznar-Sánchez, J.A., Piquer-Rodríguez, M., Velasco-Muñoz, J.F., Manzano-Agugliaro, F. (2019). Worldwide research trends on sustainable land use in agriculture. *Land Use Policy*, 87, 104069, 1–15. DOI: 10.1016/j.landusepol.2019.104069
- Camille, B. (2020). Poverty alleviation in China: The rise of state-sponsored corporate paternalism. *China Perspect.*, 3, 47–56. DOI: 10.4000/chinaperspectives.10456
- Coll, C., Galve, J.M., Sanchez, J.M., Caselles, V. (2010). Validation of landsat-7/ETM+ thermal-band calibration and atmospheric correction with ground-based measurements. *IEEE T Geosci Remote*, 48 (1), 547–555. DOI: 10.1109/TGRS.2009.2024934
- Chen, Z., Kong, F., Zhang, M. (2022). A case study of the “7–20” extreme rainfall and flooding event in Zhengzhou, Henan Province, China from the perspective of fragmentation. *Water*, 14(19), 2970. DOI: 10.3390/w14192970

- Cao, X., Liu, Y., Li, T., et al. (2019). Analysis of spatial pattern evolution and influencing factors of regional land use efficiency in China based on ESDA-GWR. *Sci Rep*, 9, 520. DOI: 10.1038/s41598-018-36368-2
- Congalton, R.G. (1991). A review of assessing the accuracy of classifications of remotely sensed data. *Remote Sens. of Environ.*, 37(1), 35–46.
- Değermenci, A.S. (2023). Spatio-temporal change analysis and prediction of land use and land cover changes using CA-ANN model. *Environ Monit Assess*, 195, 1229. DOI: 10.1007/s10661-023-11848-9
- FAO (Food and Agricultural Organization) (2020). Land use in agriculture by the numbers. <https://www.fao.org/sustainability/news/detail/en/c/1274219/> (accessed: January 9, 2024).
- Gao, B., Yang, J., Chen, Z., et al. (2023). Causal inference from cross-sectional earth system data with geographical convergent cross mapping. *Nat Commun.*, 14, 5875. DOI: 10.1038/s41467-023-41619-6
- Girma, R., Fürst, C., Moges, A. (2021). Land use land cover change modeling by integrating artificial neural network with cellular Automata-Markov chain model in Gidabo river basin, main Ethiopian rift. *Environmental Challenges*, 6, 100419. DOI: 10.1016/j.envc.2021.100419
- Godfray, H.C.J., Garnett, T. (2014). Food security and sustainable intensification. *Phil. Trans. R. Soc. B.*, 369 (1639). DOI: 10.1098/rstb.2012.0273
- Hagan, D.F.T., Wang, G., San Liang, X., Dolman, H.A.J. (2019). A time-varying causality formalism based on the Liang–Kleeman information flow for analyzing directed interactions in nonstationary climate systems. *J. Clim.*, 32(21), 7521–7537. DOI: 10.1175/JCLI-D-18-0881.1
- HPBS (Henan Province Bureau of Statistics) (2018). Statistical Yearbook of Henan Province. China Statistics Press, China. (in Chinese). <https://tjj.henan.gov.cn/2018/02-27/1373044.html> (accessed: July 18, 2023).
- Hsu, P., Xie, J., Lee, J., Zhu, Z., Li, Y., Chen, B., Zhang, S. (2023). Multiscale interactions driving the devastating floods in Henan Province, China during July 2021. *Weather. Clim. Extremes*, 39, 100541. DOI: 10.1016/j.wace.2022.100541
- Huang, D., Huang, J., Liu, T. (2019). Delimiting urban growth boundaries using the CLUE-S model with village administrative boundaries. *Land Use Policy*, 82, 422–435. DOI: 10.1016/j.landusepol.2018.12.028
- Hinz, R., Sulser, T.B., Huefner, R., Mason-D’Croz, D., Dunston, S., Nautiyal, S., et al. (2020). Agricultural development and land use change in India: A scenario analysis of trade-offs between UN Sustainable Development Goals (SDGs). *Earth’s Future*, 8, e2019EF001287. DOI: 10.1029/2019EF001287
- Jin, K., Wang, F., Zong, Q., Qin, P., Liu, C. (2020). Impact of variations in vegetation on surface temperature change over the Chinese Loess Plateau. *Sci. Total Environ.*, 716, 136967. DOI: 10.1016/j.scitotenv.2020.136967
- Kanianska, R. (2016). Agriculture and its impact on land-use, environment and ecosystem services. *IntechOpen*, 1–25. DOI: 10.5772/63719
- Li, C., Li, F., Wu, Z., Cheng, J. (2017). Exploring spatially varying and scale-dependent relationships between soil contamination and landscape patterns using geographically weighted regression. *Appl. Geogr.*, 82, 101–114. DOI: 10.1016/j.apgeog.2017.03.007
- Li, B., Cao, X., Xu, J., Wang, W., Ouyang, S., Liu, D. (2021). Spatial-temporal pattern and influence factors of land used for transportation at the county level since the implementation of the reform and opening-up policy in China. *Land*, 10, 833. DOI: 10.3390/land10080833
- Li, S., Qin, Z., Zhao, S., et al. (2022). Spatiotemporal variation of land surface temperature in Henan Province of China from 2003 to 2021. *Land*, 11, 1104. DOI: 10.3390/land11071104
- Magliocca, N.R., Dhungana, P., Sink, C.D. (2023). Review of counterfactual land change modeling for causal inference in land system science. *J Land Use Sci*, 18 (1), 1–24. DOI: 10.1080/1747423X.2023.2173325
- Meyfroidt, P., de Bremond, A., Ryan, C.M., Archer, E., Aspinall, R., Chhabra, A., et al. (2022). Ten facts about land systems for sustainability. *Proc. Natl. Acad. of Sci. U.S.A.*, 119(7). DOI: 10.1073/PNAS.2109217118
- Mu, B., Mayer, A.L., He, R., Tian, G. (2016). Land use dynamics and policy implications in Central China: A case study of Zhengzhou. *Cities*, 58, 39–49. DOI: 10.1016/j.cities.2016.05.012
- Okrah, A., Prempeh, N.A., Mensah, C., John, R., Kumi, N., Otu-Larbi, F., Kyere-Boateng, R. (2020). Impact of spatio-temporal land cover changes on land surface temperature over Dormaa from 1990–2020. *North American Academic Research*, 6(4), 87–104. DOI: 10.5281/zenodo.7838837
- Reay, D.S. (2020). Land use and agriculture: Pitfalls and precautions on the road to net zero. *Front. Clim.*, 2, 4. DOI: 10.3389/fclim.2020.00004
- Sakieh, Y., Salmanmahiny, A. (2016). Performance assessment of geospatial simulation models of land-use change – A landscape metric-based approach. *Environ Monit Assess*, 188, 169. DOI: 10.1007/s10661-016-5179-5

- Sarfo, I., Shuoben, B., Beibei, L., et al. (2022). Spatiotemporal development of land use systems, influences and climate variability in Southwestern Ghana (1970–2020). *Environ Dev Sustain*, 24, 9851–9883. DOI: 10.1007/s10668-021-01848-5
- Turner, B.L., Meyfroidt, P., Kuemmerle, T., Müller, D., Chowdhury, R. (2020). Framing the search for a theory of land use. *J Land Use Sci*, 15(4), 489–508. DOI: 10.1080/1747423X.2020.1811792
- Ullah, S., Ahmad, K., Sajjad, R.U., Abbasi, A.M., Nazeer, A., Tahir, A.A. (2019). Analysis and simulation of land cover changes and their impacts on land surface temperature in a lower Himalayan region. *Journal of Environmental Management*, 245, 348–357. DOI: 10.1016/j.jenvman.2019.05.063
- Wang, Y., Vliet, J.V., Debonne, N., Pu, L., Verburg, P. (2021). Settlements changes after peak population: Land systems projections for China until 2050. *Landsc Urban Plan*, 209, 1–12. DOI: 10.1016/j.landurbplan.2021.104045
- Xi, J., Zhou, R., Bu, R., Na, R., Guo, E. (2023). Analysis of the causal relationship between the spatial change of cultivated land conversion and economic development in North China, using Hohhot City in Inner Mongolia as an example. *Pol. J. Environ. Stud.*, 32 (4), 3373–3383. DOI: 10.15244/pjoes/162548
- Xu, D., Zhang, K., Cao, L., Guan, X., Zhang, H. (2022). Driving forces and prediction of urban land use change based on the geodetector and CA-Markov model: A case study of Zhengzhou, China. *Int. J. Digit*, 15, 1, 2246–2267. DOI: 10.1080/17538947.2022.2147229
- Yang, Q., Huang, X., Li, J. (2017). Assessing the relationship between surface urban heat islands and landscape patterns across climatic zones in China. *Scientific Reports*, 7, 9337. DOI: 10.1038/s41598-017-09628-w
- Zhao, H., Chang, J., Havlík, P., et al. (2021). China's future food demand and its implications for trade and environment. *Nat Sustain*, 4, 1042–1051. DOI: 10.1038/s41893-021-00784-6

ABSTRAKT

ZALEŻNOŚCI PRZYCZYNOWO-SKUTKOWE I PRZEWIDYWANIE SYSTEMÓW UŻYTKOWANIA GRUNTÓW W KRAJOBRAZACH WIEJSKICH: PRZYKŁADY Z PROWINCJI HENAN

Cel pracy

W rozwoju obszarów wiejskich i rolnictwa grunty odgrywają kluczową rolę w kontekście zwiększania produktywności. Aby zrozumieć wpływ konkretnych czynników (przyczyn) lub kombinacji czynników na wyniki, istotne jest zidentyfikowanie i ustalenie wyraźnych związków przyczynowych. W naszych badaniach analizujemy związki przyczynowo-skutkowe pomiędzy różnymi systemami użytkowania gruntów a temperaturą powierzchni ziemi (LST) w prowincji Henan. Ponadto opracowujemy prognozy użytkowania gruntów w oparciu o obserwowane na bieżąco trendy. Zrozumienie tej dynamiki jest niezbędne do poprawy stopnia informatyzacji rolnictwa, lepszego zarządzania środowiskiem i inteligentnych wyborów, korzystnych dla klimatu – w lokalnych okręgach, powiatach i wioskach, w ważnych rolniczo regionach Chin i poza nimi.

Materiał i metody

W badaniu wykorzystano zintegrowane dane, techniki teledetekcji i podejście przyczynowo-skutkowe do zbadania systemów użytkowania gruntów LUS i LST w prowincji Henan. Następnie zaś Moduły do Oceny Zmiany Użytkowania Gruntów (MOLUSCE) oraz automaty komórkowe – sztuczną sieć neuronową (CA-ANN), aby przewidzieć, jak będą się kształtować systemy LUS w najbliższej przyszłości (2023–2053).

Wyniki i wnioski

Wyniki badań wskazują, że tereny zabudowane (+500%), lasy (+50,88%) i zbiorniki wodne (+83,56%) znacznie powiększyły swoją powierzchnię w ciągu ostatnich 40 lat. Jednocześnie powierzchnia obszarów uprawnych (–20,81%) i jałowych (–60,53%) stale spada. Analiza wnioskowania czasowego wykazała silną zbieżność między udziałem obszarów zabudowanych a temperaturą powierzchni gruntu (LST), co potwierdza głęboki wpływ zabudowy na intensywność LST. Analiza przestrzennych wnioskowań przyczynowych pokazuje pozytywną korelację – od umiarkowanej do silnej – w zakresie pośrednich powiązań mapowania

między terenami zabudowanymi ($\rho = 0,63$) i nieużytkami ($\rho = 0,32$) w odniesieniu do LST. Prognozy dotyczące użytkowania gruntów (2023–2053) wskazują na zmniejszenie powierzchni lasów i zbiorników wodnych, zaś odwrotną tendencję w przypadku gruntów uprawnych. Informacje te są szczególnie ważne przy formułowaniu ukierunkowanych dyrektyw politycznych niezbędnych do uregulowania zaburzonej równowagi procesów użytkowania gruntów i unikania niepożądanych kompromisów gospodarczych.

Słowa kluczowe: analiza przyczynowo-skutkowa, geodetektor, użytkowanie gruntów i pokrycie terenu, temperatura powierzchni lądu (LST), Chiny

APPENDIX

Table A.1. Description of land cover types identified in Henan Province (source: Authors’ own elaboration)

Class	Definition
Forests	Closely interwoven trees and lush vegetation dominate these areas. It also includes all vegetative regions with no exposed soil.
Built-up areas	Urban, business, and industrial regions. This category also includes community green spaces, playing fields, and truck terminals.
Bare land	Bare sections of soil or rocks that have not been covered by greenery. In and around built-up regions, barren areas are noticeable. It constitutes terrains that have been cleared in preparation for redevelopment or cultivation.
Farmlands and shrubs	Widely distributed trees, hedges or bushes, secluded thickets, and non-tree crops.
Water bodies	Rivers, lagoons, lakes, and other bodies of water are all part of this ecosystem.

Table A.2 presents k_1 and k_2 becoming coefficients determined by effective wavelength of a satellite sensor based on these constants.

Table A.2. ETM+ and TM thermal band calibration constants (source: according to Coll, 2010)

	K_1 ($Wm^{-2} sr^{-1} \mu m^{-1}$)	k_2 (Kelvin)
Landsat 5 –TM	607.76	1260.56
Landsat 7 –ETM+	666.09	1282.71

Conversion of Spectral radiance (L_λ) to Kelvin with emissivity value from Landsat 8

Removal of atmospheric distortions from the thermal infrared data was performed using ENVI 5.0 software for the correction of thermal band 10 (Table A.3).

Table A.3. Band 10’s thermal constants (source: Avdan and Jovanovska, 2016)

K_1	1321.08
K_2	777.89

COMPUTATION OF REMOTELY-SENSED INDICES

Enhanced Vegetation Index (EVI)

Synonymous to Normalized Difference Vegetation Index (NDVI) is the EVI, used to quantify vegetation greenness. However, EVI elaborates by making further corrections to some atmospheric conditions and canopy background noise, which are more sensitive in areas with dense vegetation. It incorporates an “L” value to adjust for canopy background, “C” values

as coefficients for atmospheric resistance, and values from the blue band (B). These enhancements allow for index calculation (Eqn. S1) as a ratio between the R and NIR values, while reducing the background noise, atmospheric noise, and saturation in most cases:

$$EVI = G \times \frac{NIR - R}{NIR + C_1 \times R - C_2 \times B + L} \dots \quad (S1)$$

Where:

- G – gain factor (set at 2.5),
- C_1 and C_2 – correct for aerosol resistance (set at 6 and 7.5, respectively),
- L – adjusts for canopy background (set at one),
- NIR , red and blue – reflectance in the near-infrared, red and blue wavelengths, respectively.

The gain factor (G), C_1 , C_2 , and L coefficients were all derived and optimized for the MODIS sensor on the Terra and Aqua Satellites. Here, EVI is measured as in Eqn. S2:

$$EVI = 2.5 \times \frac{(Band_4 - Band_3)}{(Band_4 + 6 \times Band_3 - 7.5 \times Band_1 + 1)} \dots \quad (S2)$$

Normalized Difference Built-Up Index (NDBI)

The NDBI is another significant index used to detect built-up areas, including urban and constructed surfaces. It utilizes reflectance values from the near-infrared (NIR) and short-wave infrared (SWIR) bands.

$$NDBI = \frac{(SWIR - NIR)}{(SWIR + NIR)} \dots \quad (S3)$$

We computed NDBI using the expression (Eqn. S4):

$$NDBI = \frac{Band\ 5 - Band\ 4}{Band\ 5 + Band\ 4} \dots \quad (S4)$$

Normalized Difference Bareness Index (NDBal)

Similarly, NDBal is used to identify bare surfaces, including barren areas or soil using Eqn. S5:

$$NDBal = \frac{Band\ 5 - Band\ 6}{Band\ 5 + Band\ 6} \dots \quad (S5)$$

Normalized Difference Water Index (NDWI)

The NDWI is applied to examine water bodies. It takes advantage of the RS image's green and near-infrared regions. It is vulnerable to land development and results in overestimated water bodies. NDWI products, according to Xu (2007), can be used in connection to vegetation index change products in order to examine the backdrop of a zone's noticeable change. Water bodies have low reflectance. Only the visible fraction of the electromagnetic spectrum is reflected. Water tends to reflect more blue light (0.4–0.5 μm) than green light (0.5–0.6 μm) and red light (0.6–0.7 μm). Clear water has the highest reflection in the visible blue spectrum. As a result, water appears blue. In the visible spectrum, turbid water has a greater reflectivity. In the Near Infrared (NIR) and above, there is no reflectance. The following equations (Eqns. S6–S7) were used to quantify water index:

$$NDWI = \left(\frac{(NIR - SWIR)}{(NIR + SWIR)} \right) \dots \quad (S6)$$

$$MNDWI = \left(\frac{(Green - SWIR)}{(Green + SWIR)} \right) \dots \quad (S7)$$

EVI, NDBI, NDBal and NDWI values range from –1 to 1, with higher values indicating high density and lower values representing areas with least density for each class.

Landscape metrics

Contextually, supervised classification was used to categorize the land cover data into different classes. This step involves assigning each pixel or area to a specific land cover type (Ahmed et al., 2019). Depending on the study objectives, relevant land metrics like the percentage of land cover types, fragmentation indices, edge density, or diversity indices were calculated using Percentage of landscape (PLAND) (Eqn. S8) (Yang et al., 2017).

$$PLAND = 100 \times \sum_{p=a_{ip}}^m / A \dots \quad (S8)$$

where:

- m – the number of patches in the landscape for class p ;
- a_{ip} – the area of patch ip ;

A – the total landscape area, which is a measure of the proportion of the total area occupied by a particular land-use type.

These metrics facilitate the understanding of spatial distribution (Asgarian et al., 2014; Yang et al., 2017) and configuration of land cover types in the study area. The PLAND metrics signifies the proportion or relative contribution of a specific land cover class or feature in the overall landscape. It provides valuable information about the spatial distribution and dominance of different land cover types within a defined area. This metric is commonly used in environmental studies, land use planning, and landscape ecology to assess and understand the composition and structure of landscapes. While correlations serve as a useful tool in uncovering associations between variables, it is crucial to acknowledge their inherent symmetry, indicating they do not inherently indicate the direction of influence or establish causality (Hagan et al., 2019).

Pearson's correlation coefficient (r) analysis

A relationship between land metrics for different land cover types and surface temperature was determined using Pearson's correlation coefficient (r). The r coefficient was quantified using Eqn. S9:

$$r = \frac{\sum (x_i - \mu) (y_i - \delta)}{\sqrt{\sum (x_i - \mu)^2 \sum (y_i - \delta)^2}} \quad (S9)$$

where:

- r – correlation coefficient,
- x_i – values of the x-variable in the sample,
- μ – average values of the x-variable,
- y_i – values of the y-variable in the sample,
- δ – average values of the y-variable.

Correlation heatmap (Ullah et al., 2019) was further generated to visualize the relationships between the multiple variables in the dataset. It provides a visual representation of the correlation coefficients (r) between the pairs of variables, helping to identify patterns, trends, and dependencies (Okrah et al., 2020). Correlation heatmaps help to quickly identify which variables are positively or negatively correlated. Positive correlations (values close to 1) denote two vari-

ables that tend to increase or decrease simultaneously, whilst negative correlations (values close to -1) show that one variable tends to increase as the other decreases.

Convergent Cross Mapping (CCM) model for Temporal Causal Inference

Using Python-based Jupyter Notebook, we conducted Convergent Cross Mapping (CCM) to infer temporal indirect causality between LULCC variables and LST. The initial step involved transforming the time series data of the LULCC variable and LST into higher-dimensional spaces through data embedding, a crucial process for revealing the system's dynamics. Following this, we carefully selected appropriate lag parameters, including embedding dimensions and time delays, to optimize the CCM analysis. Subsequently, we applied the CCM algorithm, calculating cross-mapping values for the target variable based on the historical time series of the potential explanatory variables (i.e., for LULCC). Additionally, we computed cross-mapped values for the potential explanatory variables using the historical time series of the target variable (LST) (Gao et al., 2023).

In the presented scenario, a specific nonlinear system is explicitly defined, where X influences Y , and vice versa. The impact of X on Y is determined by a factor βy , x , while the effect of Y on X is influenced by a factor βx , y . The constants rx and ry introduce chaos to the system, with higher values leading to more unpredictable behaviour, as expressed by equations S10 and S11:

$$X(t+1) = X(t) [rx - rxXt - \beta y, yY(t)] \quad (S10)$$

$$Y(t+1) = Y(t) [ry - ryYt - \beta x, xX(t)] \quad (S11)$$

Geographical Convergent Cross Mapping (GCCM) model for Spatial Causal Inference

Furthermore, we employed Geographical Convergent Cross Mapping (GCCM) in Python (Jupyter Notebook) to evaluate the indirect causal relationships between LULCC variables and LST in a spatial context. GCCM involves generating cross-maps to visualize the interactions between the variables under investigation (Gao et al., 2023). Initially, we constructed embeddings, setting the dimension of the embeddings

as M . Subsequently, we iterated through each spatial unit, identifying its spatial lags of different orders. We then predicted Y based on X by defining a sequence of library sizes and compiling those vectors into a matrix based on their spatial orders. For each library size, we predicted Y , as illustrated in Eqn. S12, by searching for nearby points in the state space and constraining them by the library size:

$$\hat{Y}_s | M_x = \sum_{i=1}^{M+1} (w_{si} Y_{si} | M_x) \cdot \dots \quad (\text{S12})$$

where:

- s – a spatial unit at which the value of Y needs to be predicted,
- \hat{Y}_s – the prediction result,
- M – the number of dimensions of the embedding,
- si – the spatial unit used in the prediction,
- Y_{si} – the observation value at si and simultaneously the first component of a state in M_y , noted as $\psi(y, s_i)$.

Further, $\psi(y, s_i)$ is determined by its one-to-one mapping point $\psi(x, s_i)$, which is in turn one of the $M + 1$ nearest neighbours of the focal state $\psi(x, s)$ in M_x . w_{si} is the corresponding weight defined in Eqn. S13.

$$w_{si} | M_x = \frac{\text{weight}(\psi(x, s_i), \psi(x, s))}{\sum_{i=1}^{M+1} \text{weight}(\psi(x, s_i), \psi(x, s))} \dots \quad (\text{S13})$$

where $\text{weight}(*, *)$ is the weight function between two states in the shadow manifold, defined as Eqn. S14:

$$\text{weight}(\psi(x, s_i), \psi(x, s)) = \exp\left(-\frac{\text{dis}(\psi(x, s_i), \psi(x, s))}{\text{dis}(\psi(x, s_1), \psi(x, s))}\right) \quad (\text{S15})$$

where \exp is the exponential function, and $\text{dis}(*, *)$ represents the distance function between two states in the shadow manifold defined in Eqn. S16..

$$\begin{aligned} \text{dis}(\psi(x, s_i), \psi(x, s)) &= \\ &= \frac{1}{M} \left(|h_{si}(x) - h_s(x)| \sum_{k=1}^{M-1} \text{abs}[h_{si(k)}(x), h_{s(k)}(x)] \right) \end{aligned} \quad (\text{S16})$$

where $(*)$ means the absolute value of a real number, and $\text{abs}(*, *)$ represents the distance function between two vectors, as the first element $h_{si}(x)$ in $\psi(x, s_i)$ corresponds to the spatial focal units, while other elements in $\psi(x, s_i)$ respectively correspond to a vector with several spatial units.

The concrete form of $\text{abs}(*, *)$ for raster data and polygon data are specified as abs_r and abs_v in Eqn. S17 and Eqn. S18, respectively.

$$\begin{aligned} \text{abs}_r[h_{si(k)}(x), h_{s(k)}(x)] &= \\ &= \frac{1}{D} \sum_d |u_{si(k,d)}(x) - u_{s(k,d)}(x)| \end{aligned} \quad (\text{S17})$$

$$\begin{aligned} \text{abs}_v[h_{si(k)}(x), h_{s(k)}(x)] &= \\ &= \left| \frac{1}{D_1} \sum_d^{D_1} u_{si(k,d)}(x) - \frac{1}{D_2} \sum_d^{D_2} u_{s(k,d)}(x) \right| \end{aligned} \quad (\text{S18})$$

where:

- $u_{si(k,d)}(x)$ – the spatial unit of the k th-order spatial lags of si in the direction d ,
- D – the number of spatial units (or directions) in the k th-order,

The skill of cross-mapping prediction is measured by the Pearson correlation coefficient between the true observations and corresponding predictions, defined in Eqn. S19.

$$\rho = \frac{\text{Cov}(Y, \hat{Y})}{\sqrt{\text{Var}(Y) \text{Var}(\hat{Y})}} \quad (\text{S19})$$

where $\text{Cov}(Y, \hat{Y})$ represents covariance, and $\text{Var}(Y, \hat{Y})$ represents variance.

We further examined the cross-maps to identify patterns of convergence, searched for consistent patterns in which changes in LULCC variables (causes) precede changes in LST intensity (effects).

Other findings

Rural and urban dynamics in Henan Province

Figure S1 depicts spatial distribution, and Figure S2 illustrates trends of rural and urban settings over the

past 40 years in the studied domain. The illustrations present area changes pertaining to the spatial distribution of the region’s rurality and urbanism. Spatial analysis shows urban areas have been on ascendancy, having expanded from 415.70 km² in 1983 to 8,656.57 km² (2023). Surprisingly, rural areas have undergone constant fluctuations over the same period. A spike in rural areas’ trajectory could be observed between 1993 (1, 281.16 km²) and 2013 (2,221.52 km²), followed by a sharp decline in 2023 (1,775.33 km²) which can be attributed to some socio-political and economically or policy-driven factors.

Dark red spots indicate high-density urban concentration hotspots like Zhengzhou, Huanglongsi, Shangqiu, Luoyang, Nanyang, Xinyang, Xinxiang,

Anyang, etc. Rural or low-density urban concentration zones are characterized by light green patches, located around southern and western parts of Henan Province. Rural areas are predominated by economic activities such as granary/agriculture and industrial activities, and are mostly characterized by elevation, terrain/slope, aspects and water bodies in the aforementioned areas.

Land metrics and LST

Statistical interpretations of land metrics/PLAND analysis show quite a significant inverse correlation ($-0.63, p < 0.05$) between farmlands/shrubs (i.e., crops, orchards, thickets, etc.) and LST (Fig. S3). Here, farmlands/shrubs obtained 46.1% coverage. As

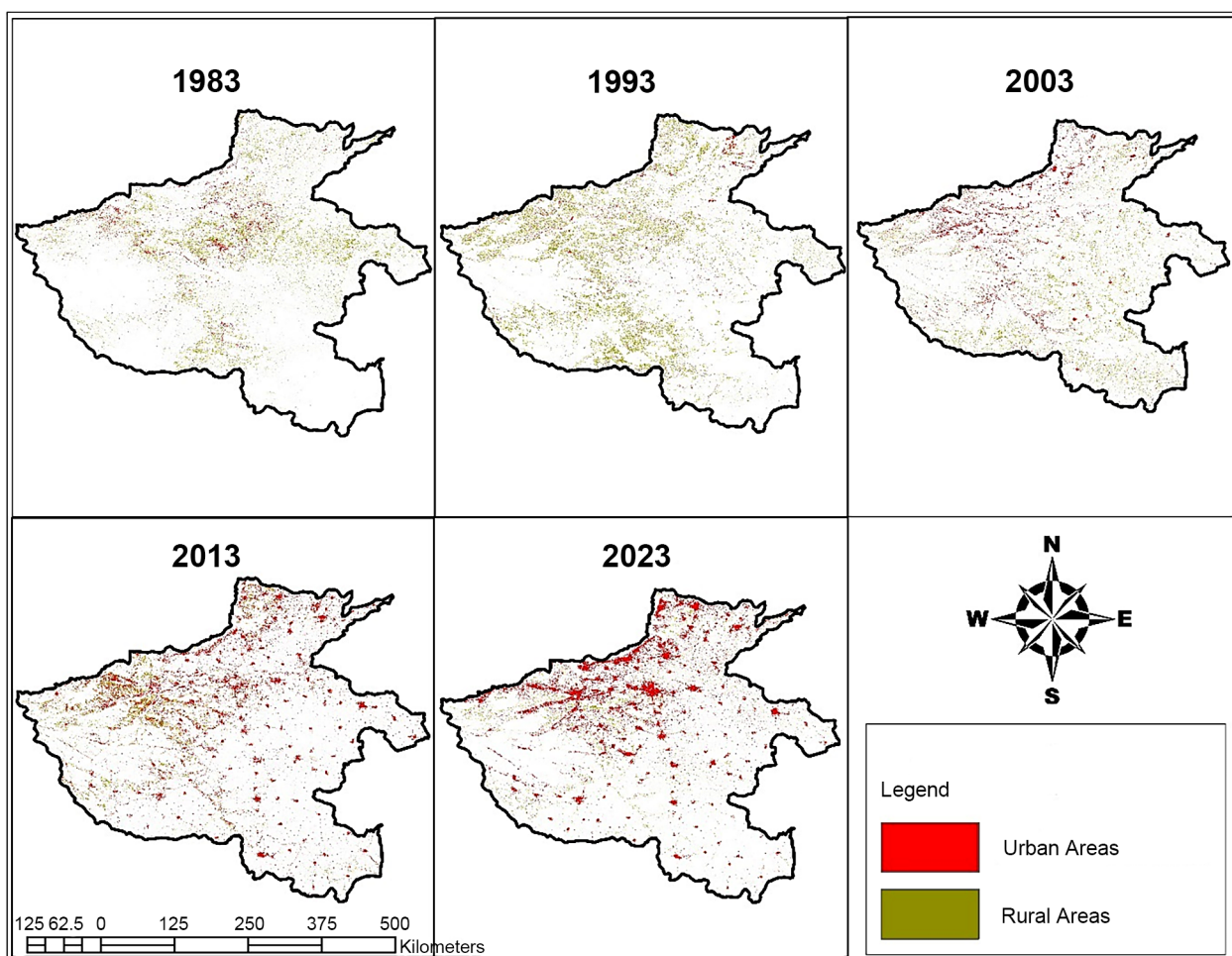


Fig. S1. Spatial distribution of Henan Province’s rural and urban areas (source: Authors’ own elaboration)

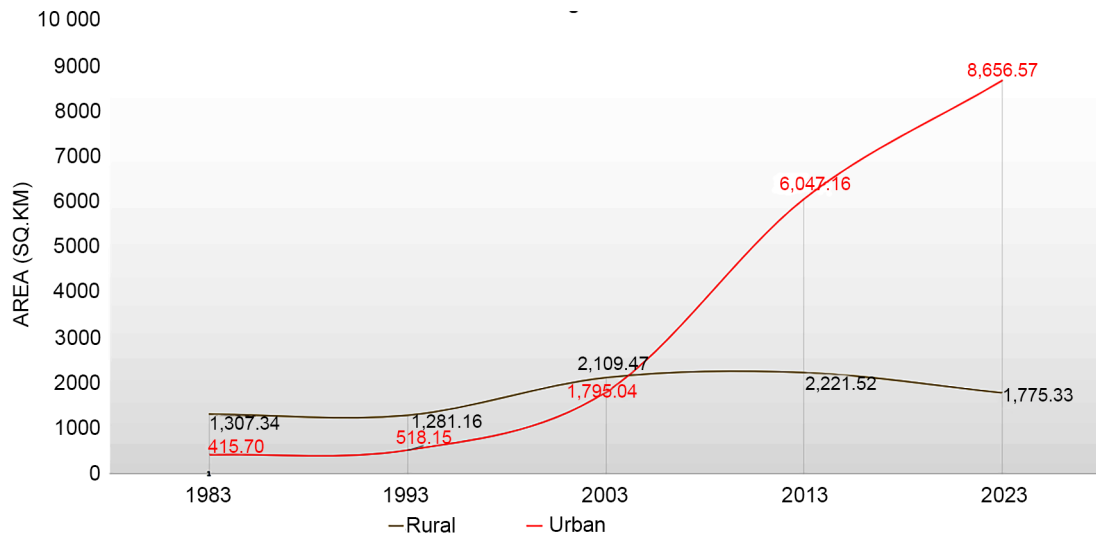


Fig. S2. Spatial trends in Henan Province's rural and urban areas over the past 40 years (source: Authors' own elaboration)

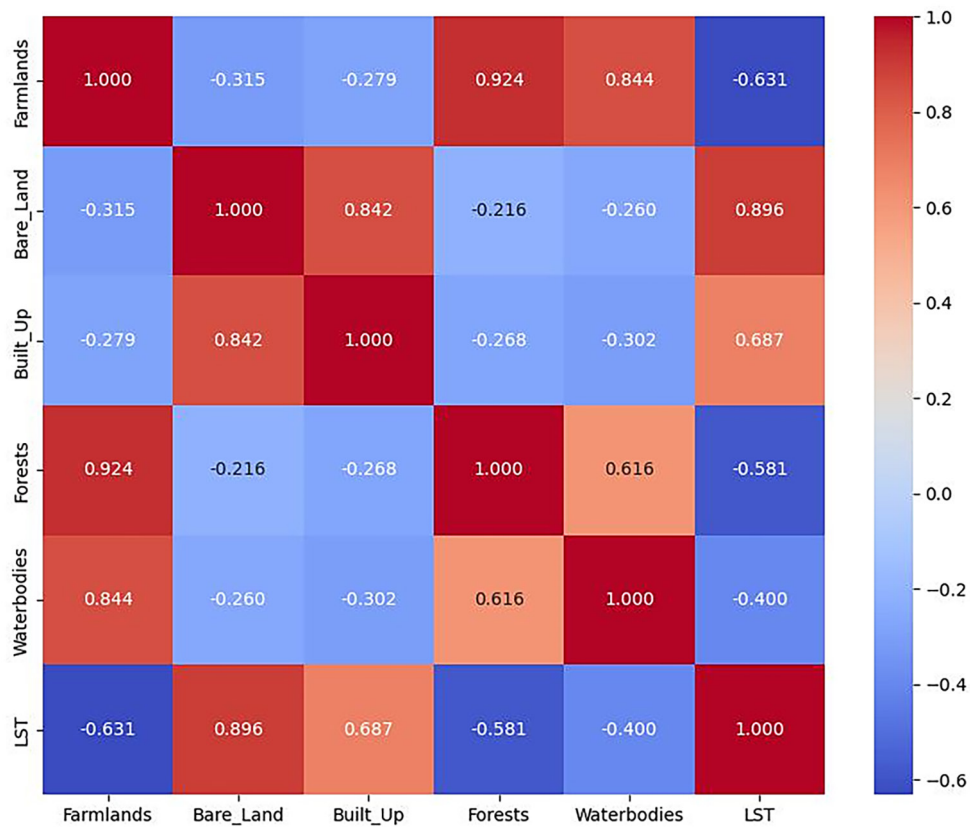


Fig. S3. Correlation analysis between the understudied land cover types and surface temperature (source: Authors' own elaboration)

the percentage of farmlands/shrubs declines, surface temperature amplifies. Agricultural practices could be designed to optimize cooling effects by promoting agroforestry, i.e. green alternative livelihood projects that do not adversely impact the forests. By considering the impacts of land cover on local LST, policymakers and stakeholders can make informed decisions to create more sustainable and climate-friendly environments. A moderate negative correlation (-0.58 , $p < 0.05$) was generated for forests and LST. Forests covered an area of about 24.3%. Thus, expansion in forest areas resulted in the reduction of LST. Forests serve as natural LST regulators, as they minimize heat stress and create more pleasant microclimatic conditions (Asgarian et al., 2014). Additionally, a significant negative correlation (-0.4 , $p < 0.05$) was obtained for water bodies (such as lakes, rivers, or reservoirs) and LST. Areas covered by water amounted to 10.7%. These correlations demonstrate the significant influence of land cover types on prevailing LST patterns (Ahmed et al., 2019). Understanding these relationships is crucial for effective climate resilience planning and sustainable land use management, considering the physical and socio-economic characteristics of Henan Province.

Similarly, a significant positive correlation (0.9 , $p < 0.05$) between bare land and LST was obtained. Barren areas obtained a 9.2% in area coverage. Findings indicate an increment in the percentage of barren areas induce the amplification of LST. This suggests that areas with little or no vegetation, such as bare surfaces, deserts, rocky surfaces or limited greenery, may contribute to higher local temperatures, as they absorb and retain more heat/energy (Al et al., 2020). The piecemeal of evidence presented in Fig. S3, exhibits a moderate positive correlation (0.69 , $p < 0.05$) between built-up and LST. Here, built environment obtained 9.7% coverage. The results indicate the percentage of built environment amplified in tandem with LST. Findings indicate areas with high density of built-up such as Zhengzhou, Shangqiu, Anyang, Hebi, Nanyang, Xinyang, Puyang, Jianguanchi and Luohe experience higher temperatures due to their composition or land use structure, compared to areas with low density hotspots. As cities or urban areas expand, they replace natural surfaces with impervious surfaces (traditional or impermeable concretes, pavers and asphalts), which absorb and store heat, resulting in higher LST compared to the surrounding rural areas.